A Chloride-Doped Silver-Sulfide Cluster $[Ag_{148}S_{26}Cl_{30}(C{\equiv}CBu^t)_{60}]^{6+}$: Hierarchical Assembly, Enhanced Luminescence and Cytotoxicity to Cancer Cells

Table of Contents

General experimental section

UV–vis spectra were measured on an Analytik Jena S600 UV–visible spectrophotometer. PL spectra were taken on an Edinburgh Instruments FLS920 spectrometer. PL decay dynamics was recorded on a time correlated single-photon counting (TCSPC) spectrofluorometer (FLS920, Edinburgh Instrument) with a 405 nm picosecond pulsed laser at a repetition frequency of 0.2 MHz. All optical measurements were performed at room temperature. The NMR spectra were recorded on a Bruker Advance III 600 MHz instrument at room temperature, using 5 mm tubes for ^{1}H and ^{31}P. Single-crystal X-ray diffraction data was recorded on Bluker D8 VENTURE at 120 kV. Powder XRD patterns were obtained using a Bruker D8 Advance X-ray diffractometer with (λ (CuKα) = 1.5405 Å) radiation. X-ray photoelectron spectroscopy (XPS) survey was conducted by a VG multilab ESCA system. TEM image was acquired on a Hitachi 7700 transmission electron microscope at 100 kV. High resolution mass spectrometry was recorded on an Agilent 6224 (Agilent Technologies, USA) ESI-TOF-MS spectrometer. EPR was carried out on an X-band (9.5 GHz) spectrometer (Bruker A300) at 120 K. The following settings are used: 20 mW microwave power, 3000 G center field, 6000 G sweep width and 5 G field modulation.

Materials and reagents.

Tris(2-carboxyethyl)phosphine Hydrochloride and 3,3-Dimethyl-1-butyne and silver hexafluoroantimonate were purchased from Saen Chemical Technology Co., Ltd (Shanghai, China). Thionyl chloride and other reagents employed were purchased from Sinopharm Chemical Reagent Co., Ltd. (Shanghai, China). All other chemicals and solvents for synthesis were of analytical grade and used without further purification. The solvents used were of analytical grade.

HeLa, A549 and SW620 cells were purchased from the National Collection of Authenticated Cell Cultures (NCAC, China) and they were recently authenticated and tested to rule out mycoplasma contamination.

Synthesis and characterization of new template agent

Synthesis of template agent was shown in Scheme S1. Tris(2-carboxyethyl)phosphine Hydrochloride (10 mmol) was dissolved in methanol, thionyl chloride (50 mmol) was added dropwise in ice bath, then stir the reaction mixture at room temperature for 12 hours under an atmosphere. After reaction, the solution was evaporated to obtain colorless oil mixed with white solid, dichloromethane was added then was filter, filtrate was wash twice by deionized water, the organic phase was combined and evaporated to obtain a colorless oil, this crude product can be directly used to evaluate color change experiment of silver nitrate for Figure S1.

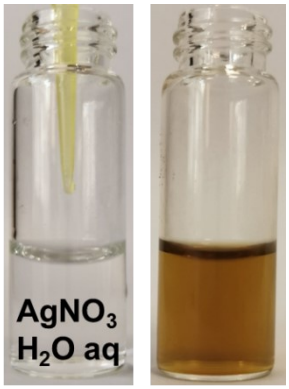

Figure S1. Photograph of $AgNO_3$ aqueous solution before and after adding new template agent.

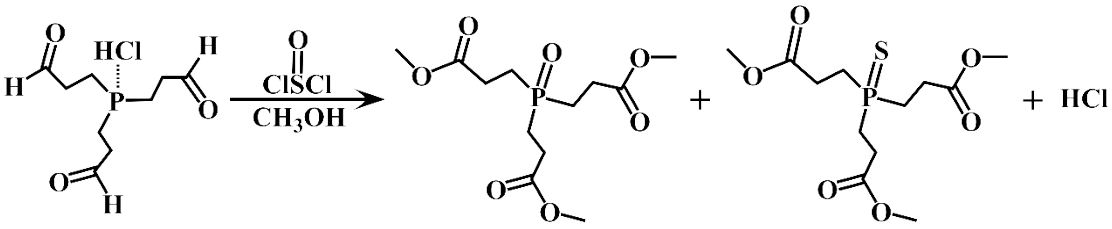

Scheme S1. The esterification reaction of tris(2-carbonylethyl)phosphorus hydrochloride.

The tertiary phosphine sulfide is responsible for the supply of template S^{2-}, which can be verified by S^{2-} releasing from triphenylphosphine sulfide.

Figure S2. The crude product with two components.

^{1}H NMR and ^{31}P NMR of template agent

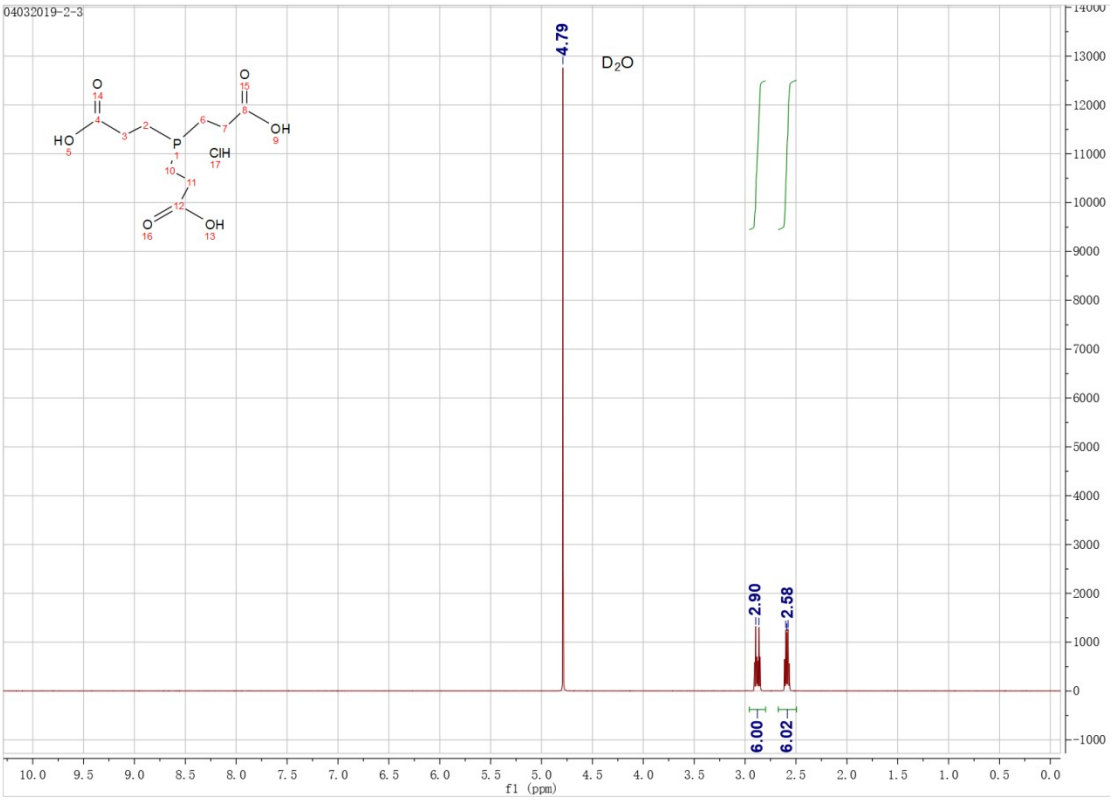

Figure S3. ^{1}H NMR of Tris(2-carboxyethyl)phosphine Hydrochloride.

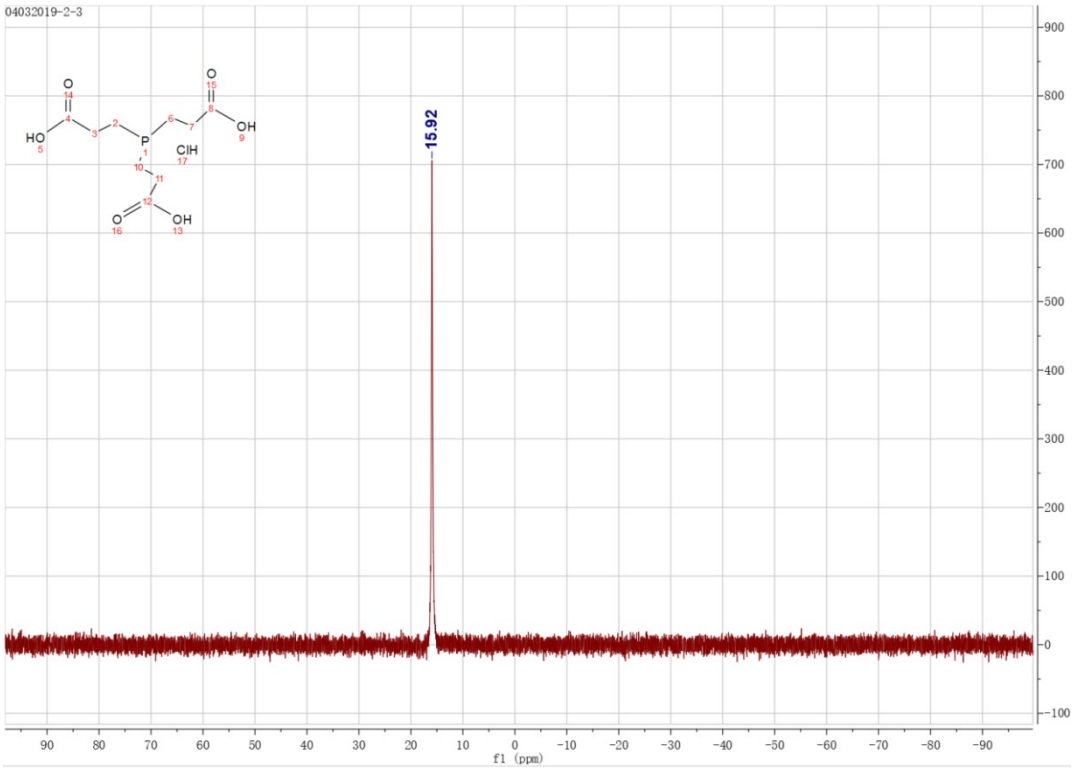

Figure S4. ^{31}P NMR of Tris(2-carboxyethyl)phosphine Hydrochloride.

Figure S5. ^{1}H NMR of the crude product.

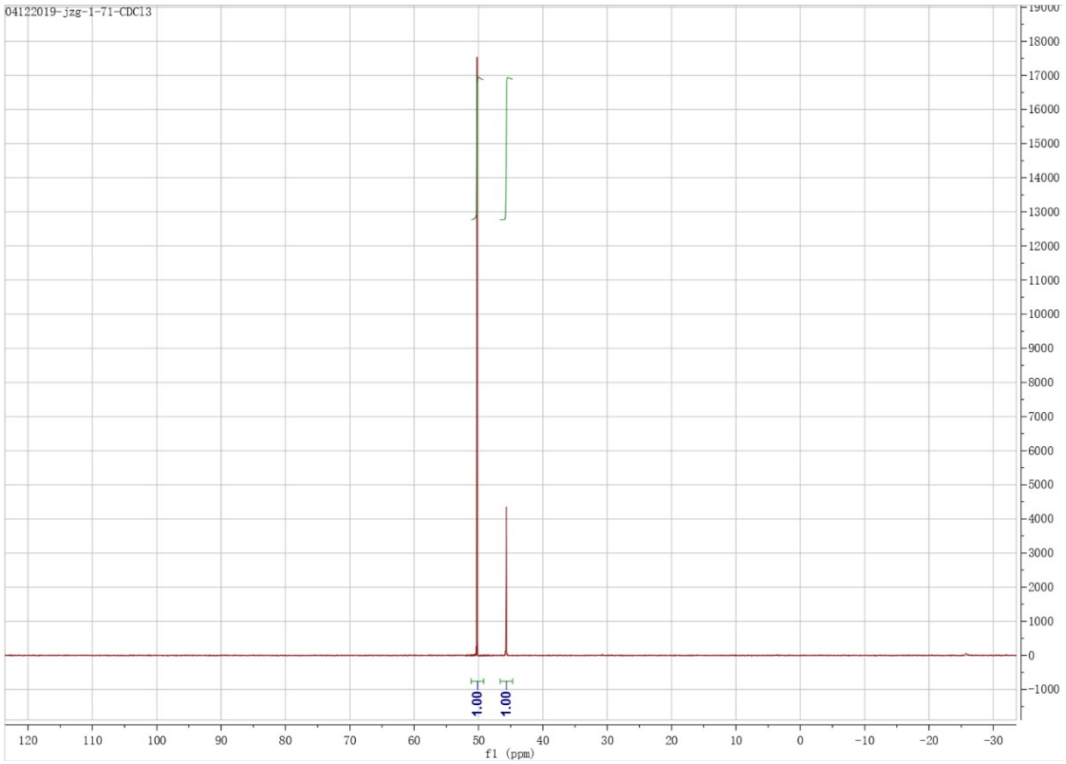

Figure S6. ^{31}P NMR of the crude product.

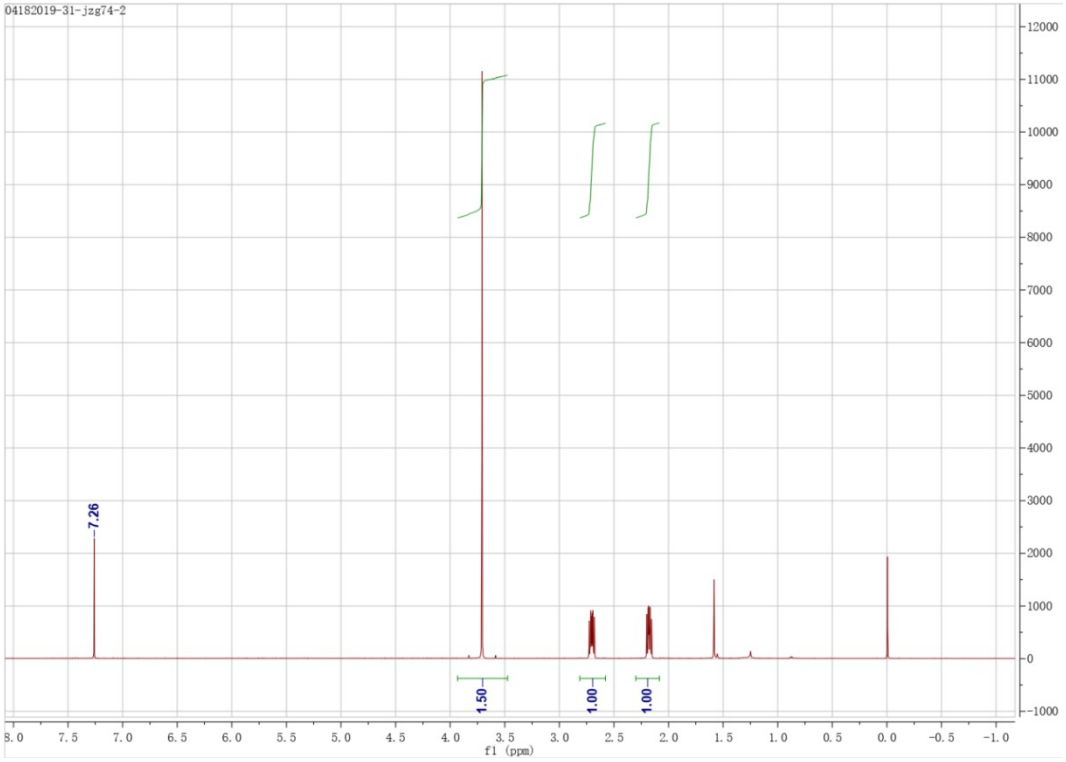

Figure S7. ^{1}H NMR of the purified product by TLC.

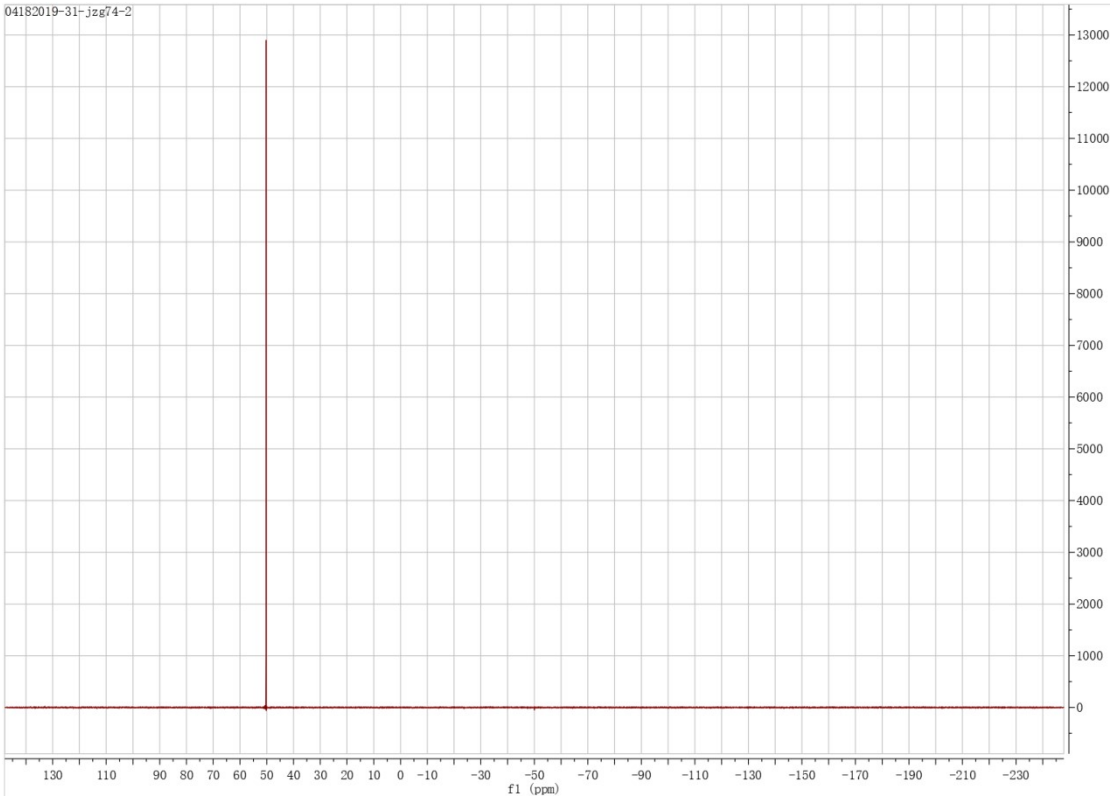

Figure S8. ^{31}P NMR of the purified product by TLC.

Gas Chromatography-Mass Spectrometry of template agent

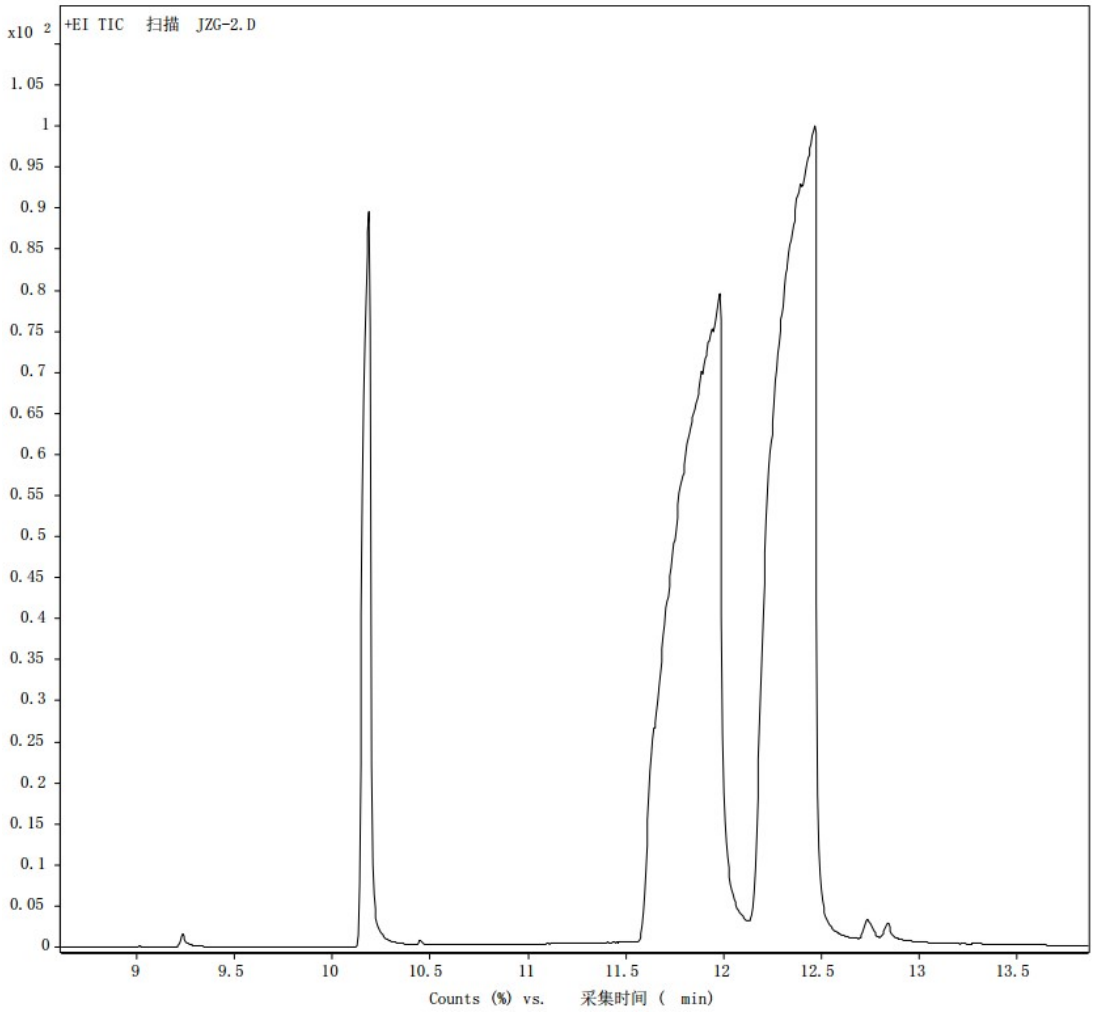

Figure S9. Gas chromatography-Mass Spectrometryof the crude product.

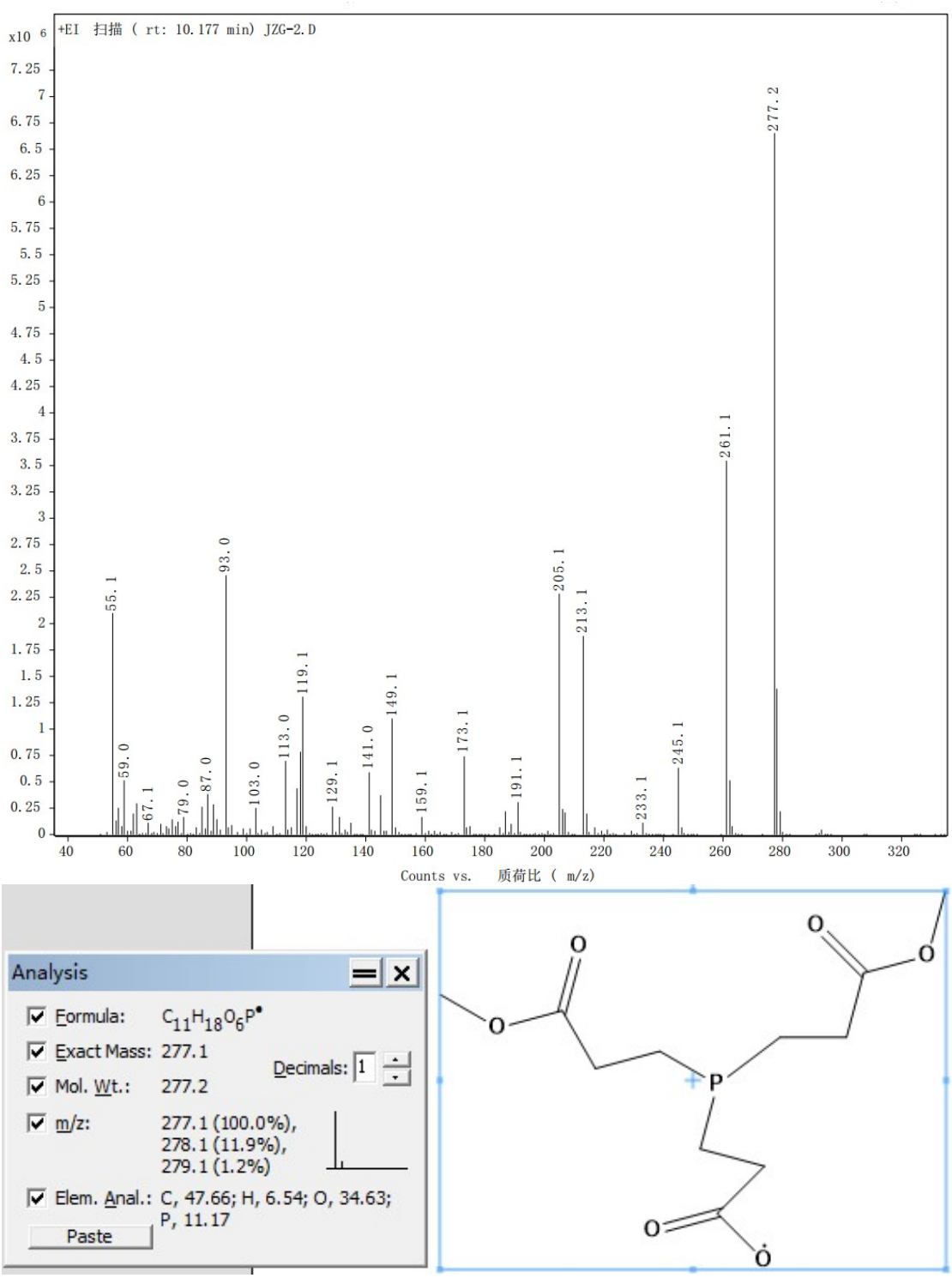

Figure S10. Mass Spectrometry of the product by chromatography at 10 min.

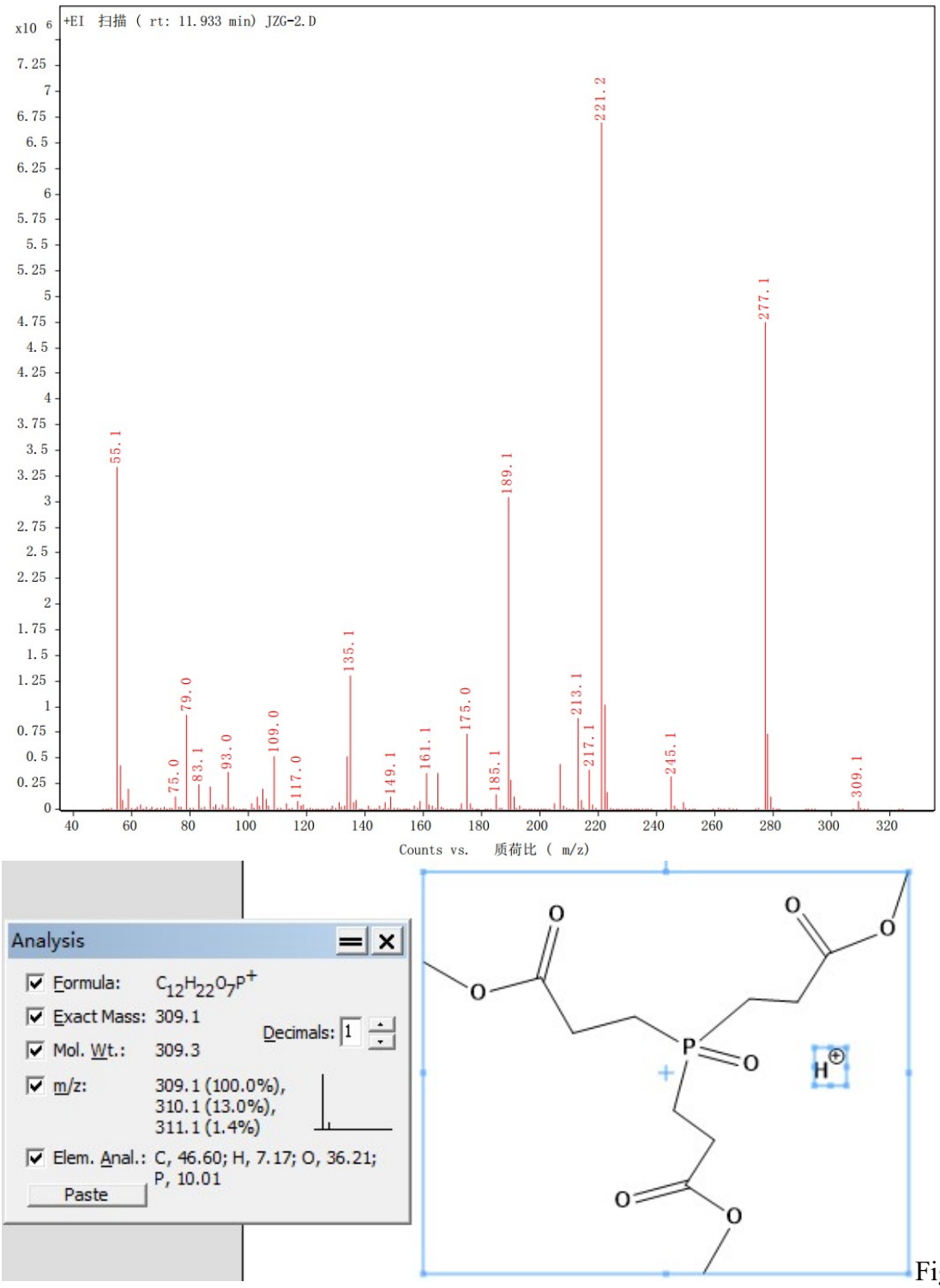

Figure S11. Mass Spectrometry of the product by chromatography at 11.9 min.

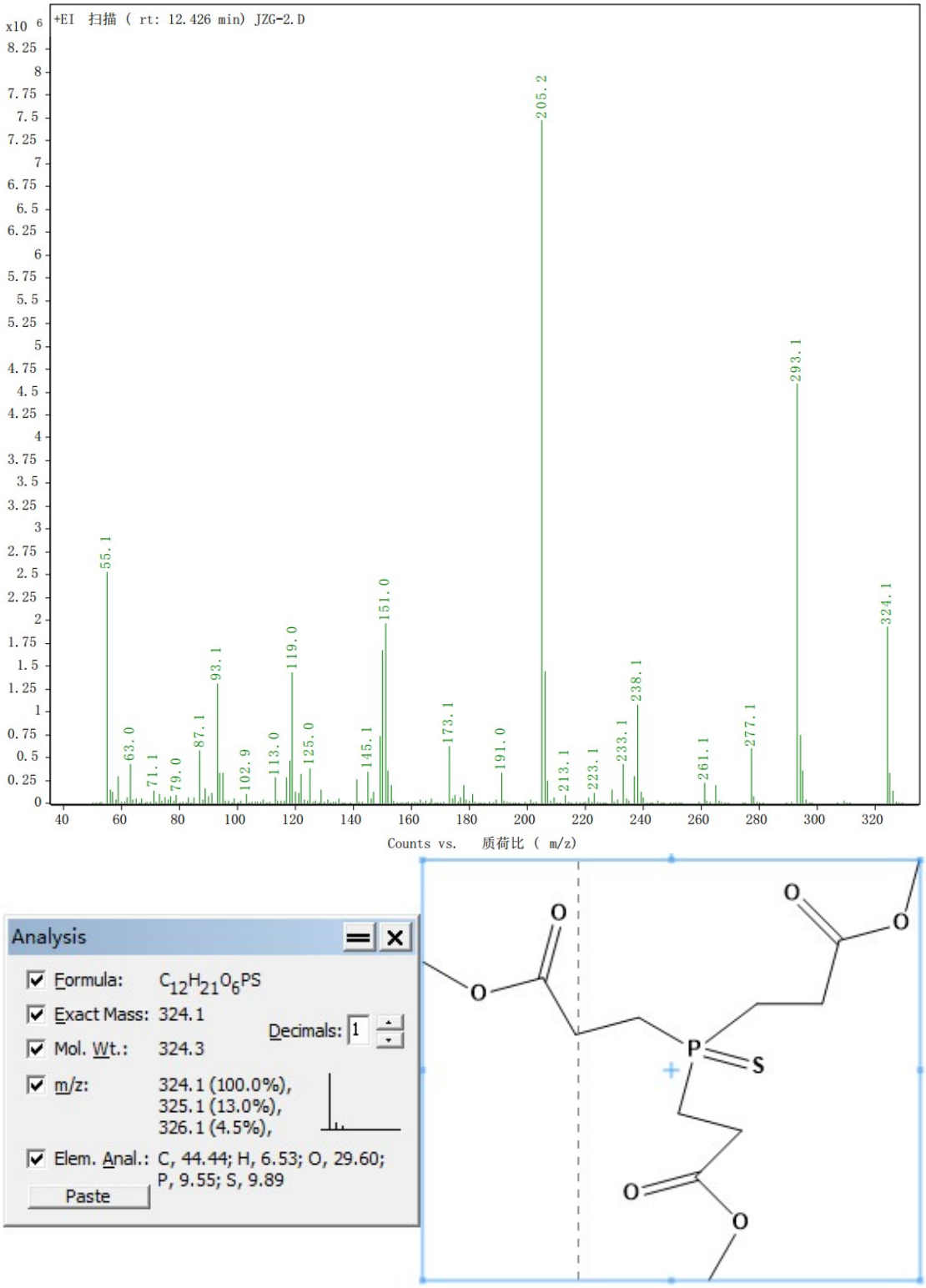

Figure S12. Mass Spectrometryof the product by chromatography at 12.4 min.

Synthesis and characterization of Ag_{148}

$\{AgC{\equiv}CBu^t\}_n$: Ag_2O (2 g, 8.6 mmol) was weighed into a 100 ml flask, and 40 ml of ammonium hydroxide was added. The solution was filtered after stirred for 5 min. 3,3-Dimethyl-1-butyne (3.8 g, 16 mmol) in 5 ml of ethanol was added to the above silver ammonia solution under stirring, and a white precipitate formed immediately, which was washed with water and dried in a vaccum desiccator at room temperature to give white $\{AgC{\equiv}CBu^t\}_n$.

$\{AgC{\equiv}CBu^t\}_n$. (0.1 mmol) and silver hexafluoroantimonate (0.2 mmol) were weighed into a 10 ml vial, and 6 ml of CH_3OH was added then ultrasound for 5 min to get a white mixture, 500 uL diluted crude template agent (200 uL + 6 mL CH_3OH) was added to get light yellow turbidity, then the mixture was stirred at room temperature until turned to the orange red solution with red emit by an ultraviolet lamp. Then the solution was filtrated and concentrated, then was added in 5 ml CH_3OH to remove insoluble components by centrifugation. After evaporation of the solvent, the red solid was collected and subjected to the diffusion of diethyl ether, red crystals deposited after about 5 days (yield 23.2% based on Ag).

Figure S13. The reaction product monitored by an ultraviolet lamp.

Powder X-ray diffraction (PXRD) of Ag_{148}

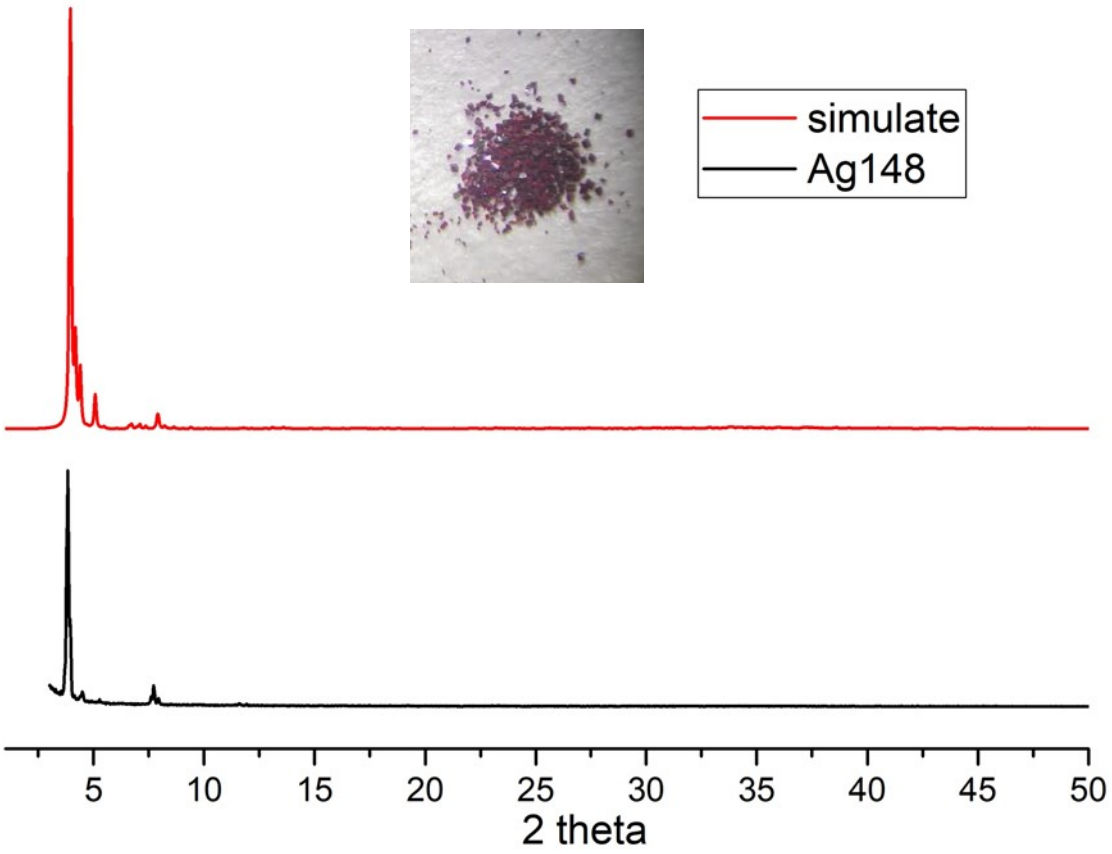

Figure S14. Experimental and simulated PXRD patterns of Ag_{148}.

Crystal data and structure refinement

Single-crystal X-ray diffraction data collection of Ag_{148} was recorded on Bluker D8 VENTURE diffractometer equipped with a PHOTON 100 CMOS bidimensional detector and MoKα monochromatized radiation (λ = 0.71073 Å) at 120 K. The structure was solved by intrinsic phasing methods and refined by full-matrix least squares using the SHELX-TL package[1,2] and OLEX 2[3].

Specific Refinement Details as follow: All Ag Cl (or S) atoms and most coordinated $CCBu^t$ ligands were located in the electron density. All heavy Ag Cl (or S) and C atoms were refined with anisotropic thermal parameters. DFIX restraints were applied to keep some bond lengths of Bu^t and counter ions in reasonable ranges. SIMU restraints were also used for all C and some disordered silver atoms. Additional counter ions of SbF_6^-, of which four Sb were refined with anisotropic thermal parameters two Sb and all F were refined with isotropic thermal parameters due to the large thermal motion or some disorder. Solvent molecules were taken into account with the SQUEEZE/PLATON procedure.

In all, despite an R_1 value that was a less than ideal and resolution that was poorer than generally obtained in crystallography of some small molecules, a reasonable quality refinement was achieved, and the current data is more than adequate for establishing the average connectivity of the structure. Crystallographic data for single-crystal X-ray diffraction studies are summarized in Table S1. Further details about of the crystal structure determinations may be obtained free of charge at http://www.ccdc.cam.ac.uk/. CCDC 2116315-2116316.

Table S1 Crystal data and structure refinement for $Ag_{148}X_{56}$ (X = Cl).

Identification code	J
Empirical formula	$C_{720}H_{1080}Ag_{296}Cl_{112}F_{72}Sb_{12}$
Formula weight	48464.70
Temperature/K	120.01
Crystal system	monoclinic
Space group	$P2_1/c$
a/Å	46.413(11)
b/Å	27.613(7)
c/Å	47.653(10)
α/°	90
β/°	108.954(4)
γ/°	90
Volume/Å^3	57760(23)
Z	2
ρ_{calc}g/cm^3	2.787
μ/mm^{-1}	5.461
F(000)	44952.0
Crystal size/mm^3	0.2 × 0.15 × 0.15
Radiation	MoKα (λ = 0.71073)
2Θ range for data collection/°	3.73 to 46.512
Index ranges	$-51 \leq h \leq 38$, $-30 \leq k \leq 16$, $-52 \leq l \leq 52$
Reflections collected	192380
Independent reflections	79016 [R_{int} = 0.0783, R_{sigma} = 0.1316]
Data/restraints/parameters	79016/7224/5586
Goodness-of-fit on F^2	1.053
Final R indexes [I>=2σ (I)]	R_1 = 0.1083, wR_2 = 0.2814
Final R indexes [all data]	R_1 = 0.1820, wR_2 = 0.3200
Largest diff. peak/hole / e Å^{-3}	3.04/-3.61

Table S2 Crystal data and structure refinement for $Ag_{148}X_{56}$ (X = S).

Identification code	J
Empirical formula	$C_{720}H_{1080}Ag_{296}F_{72}S_{112}Sb_{12}$
Formula weight	48085.02
Temperature/K	120.01
Crystal system	monoclinic
Space group	$P2_1/c$
a/Å	46.413(11)
b/Å	27.613(7)
c/Å	47.653(10)
α/°	90
β/°	108.954(4)
γ/°	90
Volume/Å^3	57760(23)
Z	2
ρ_{calc}g/cm^3	2.765
μ/mm^{-1}	5.404
F(000)	44728.0
Crystal size/mm^3	0.2 × 0.15 × 0.15
Radiation	MoKα (λ = 0.71073)
2Θ range for data collection/°	3.73 to 46.512
Index ranges	$-51 \le h \le 38$, $-30 \le k \le 16$, $-52 \le l \le 52$
Reflections collected	192380
Independent reflections	79016 [R_{int} = 0.0783, R_{sigma} = 0.1316]
Data/restraints/parameters	79016/7224/5586
Goodness-of-fit on F^2	1.048
Final R indexes [I>=2σ (I)]	R_1 = 0.1085, wR_2 = 0.2813
Final R indexes [all data]	R_1 = 0.1822, wR_2 = 0.3201
Largest diff. peak/hole / e Å^{-3}	3.00/-3.63

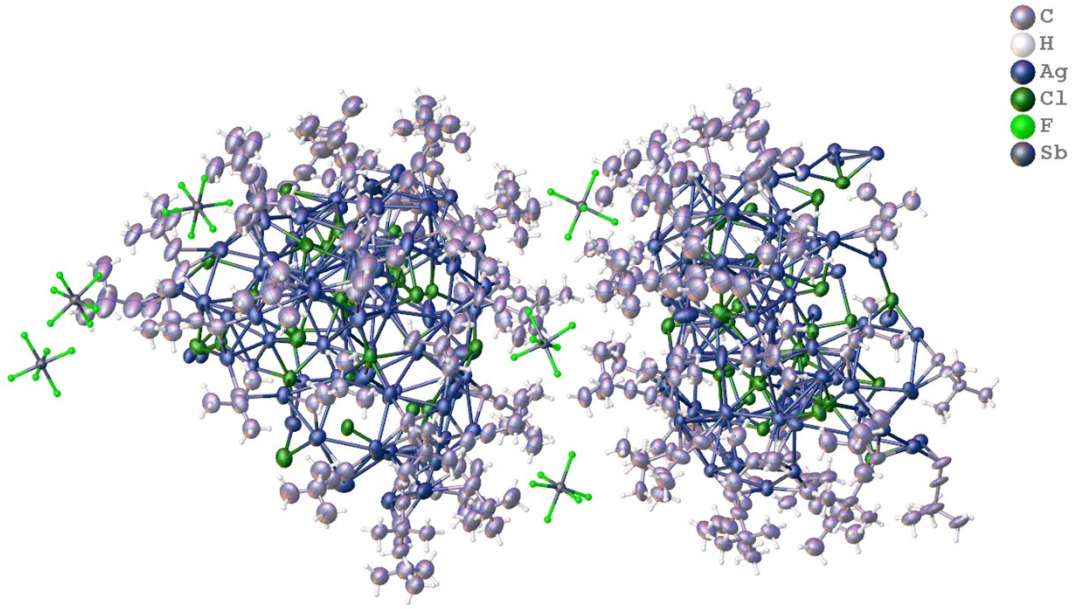

Figure S15. Two crystallographic independent $Ag_{74}Cl_{28}(C_6H_9)_{30}$ with a non-crystallographic symmetry in the OLEX2 interface.

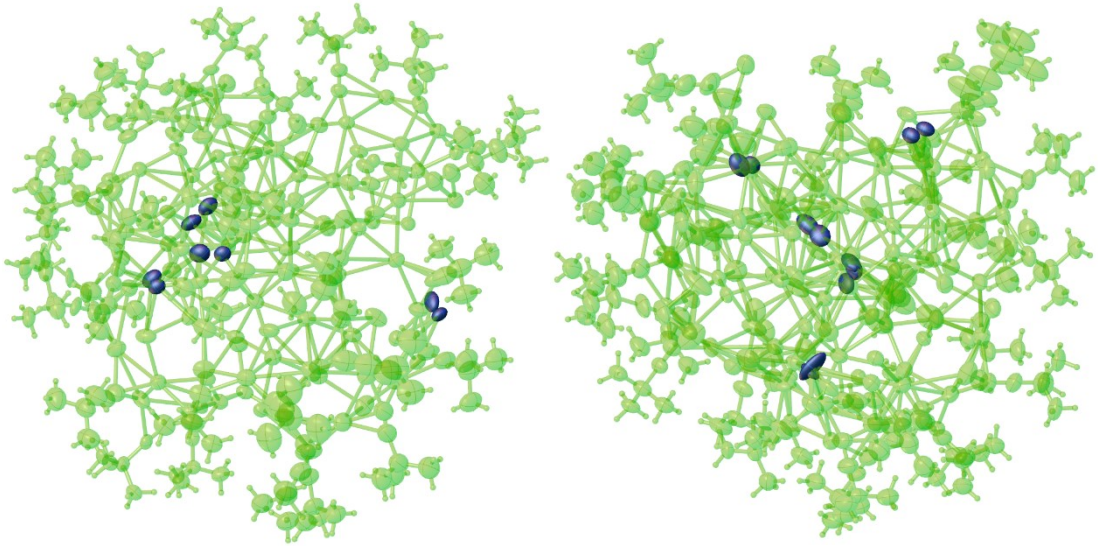

Figure S16. All Ag atoms were refined with anisotropic thermal parameters, the nine silver atoms were disordered in two positions as a result of unreasonably elongated a.d.p. ellipsoids and relatively high surrounding residual electron density.

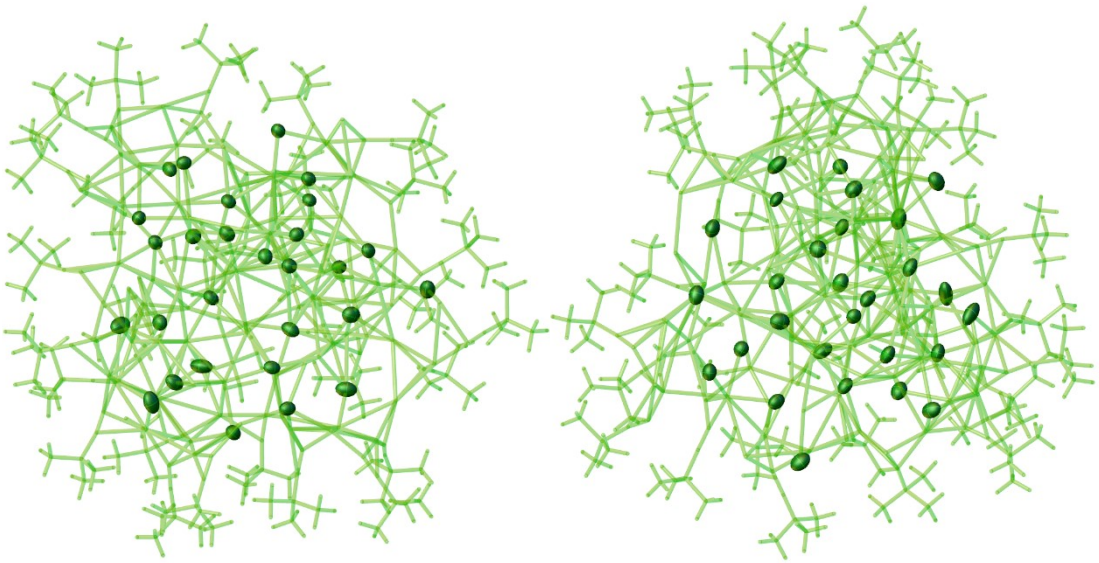

Figure S17. All Cl atoms were refined with anisotropic thermal parameters as full occupancy in the OLEX2 interface.

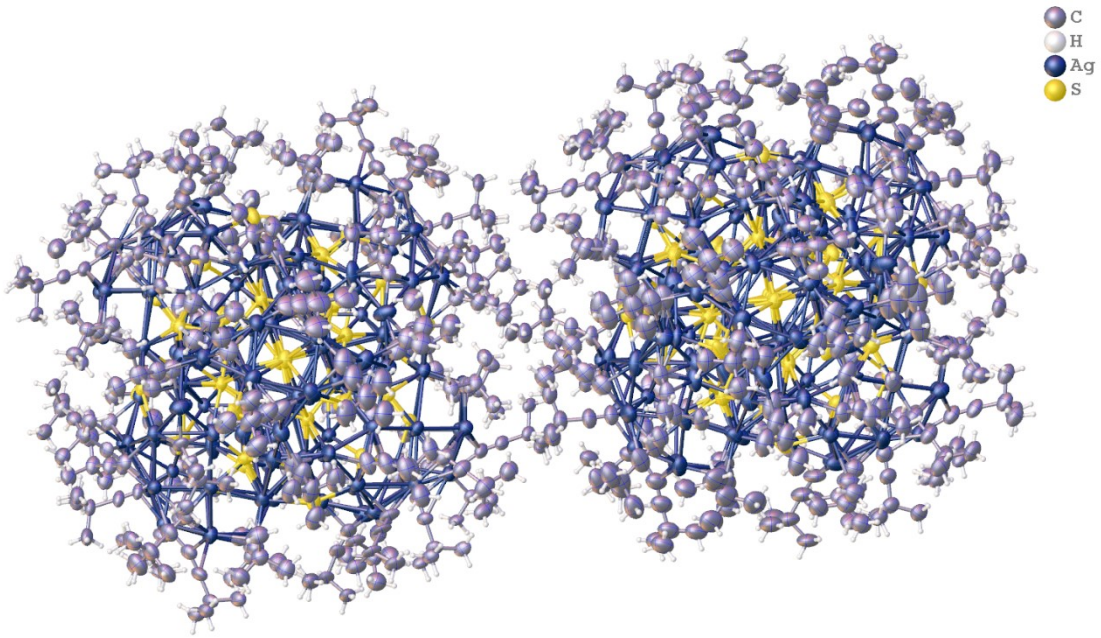

Figure S18. The structure refinement using S instead of Cl in the OLEX2 interface (grow mode), thermal displacement parameters of S and Cl and the final r-values are almost identical.

Atomic content determination of Ag_{148}

Table S3. Atomic content determination of Ag_{148}

	Ag	S	Cl	Sb
SCXRD	148	x	56-x	a
ICP-MS	148	-	-	5.8
EDX	150	23	26	5
XPS	145	32	26	8

ICP-MS of Ag_{148}

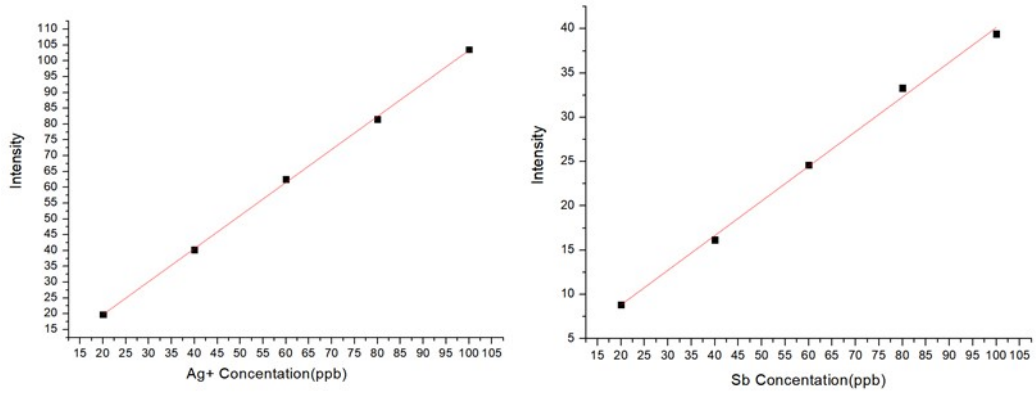

	Ag_{107}	In_{115}	Sb_{121}
SAMPLE-BLK	0.300862099	245.3%	0.250962189
$AgSbF_6$	33.20887911	194.0%	30.75590223
Ag_{148}	374.1773492	207.2%	14.71785654

EDX of Ag_{148}

Element	Weight %	Atom %
C K	49.84	86.41
Cl K	2.35	1.38
S K	1.90	1.23
Ag L	41.97	8.10
Sb L	1.57	0.27
F K	2.37	2.60

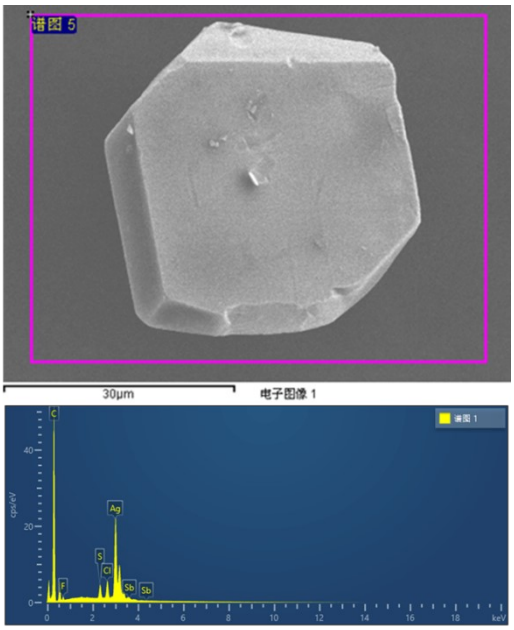

Figure S19. EDX of one crystal of Ag_{148}.

XPS of Ag_{148}

Name	Peak BE	FWHM eV	Area (P) CPS.eV	Atomic %
Cl 2p	198.65	3.22	21516.70	3.31
S 2p	162.07	3.09	18636.27	4.09
C 1s	284.80	3.01	106790.22	47.51
Ag 3d	368.69	2.66	850526.49	18.07
Sb 3d	532.02	2.82	85393.91	1.14
F 1s	685.11	2.75	47875.10	7.03

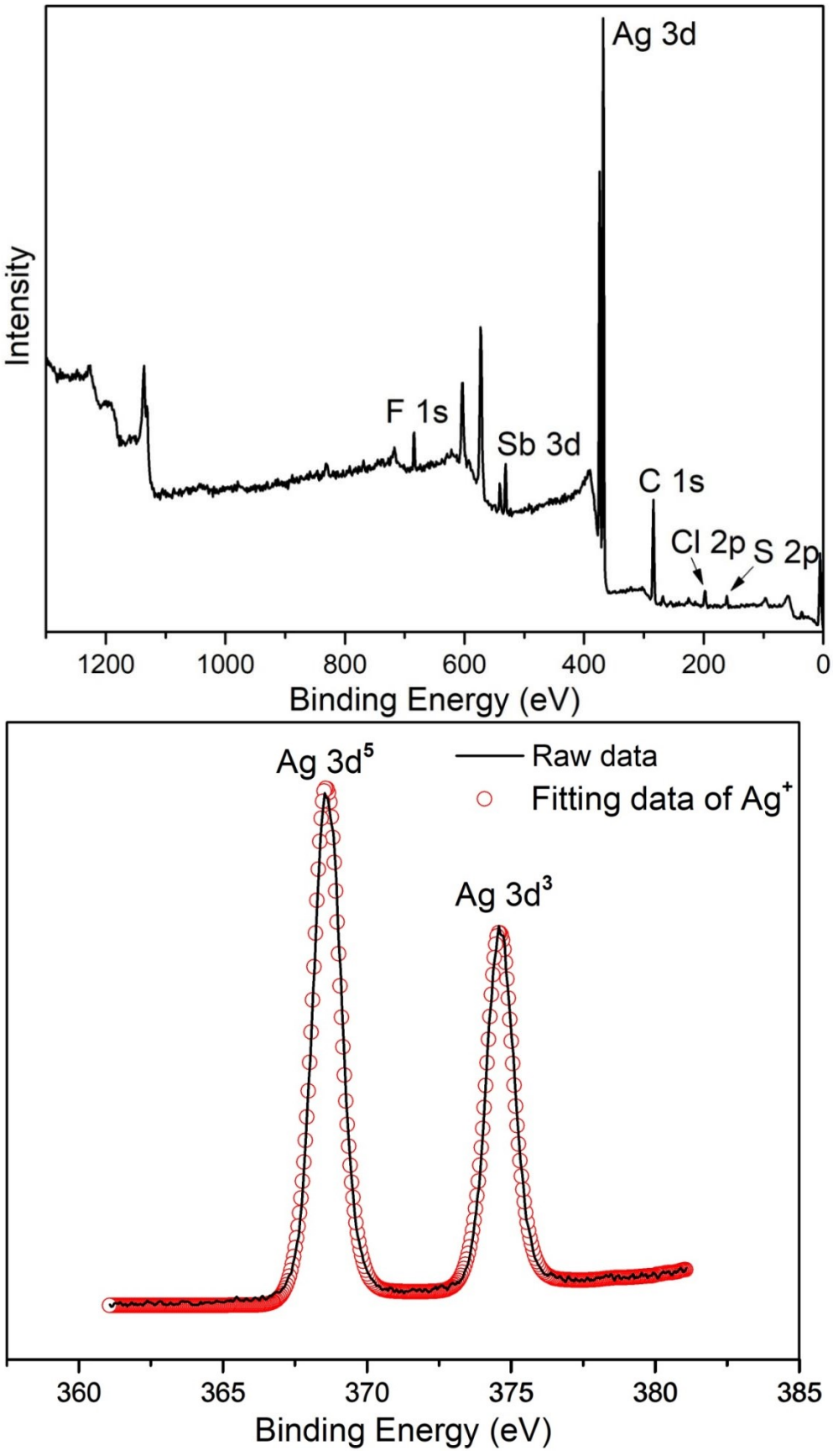

Figure S20. XPS of the crystals of Ag_{148}.

ESI-MS of Ag_{148}

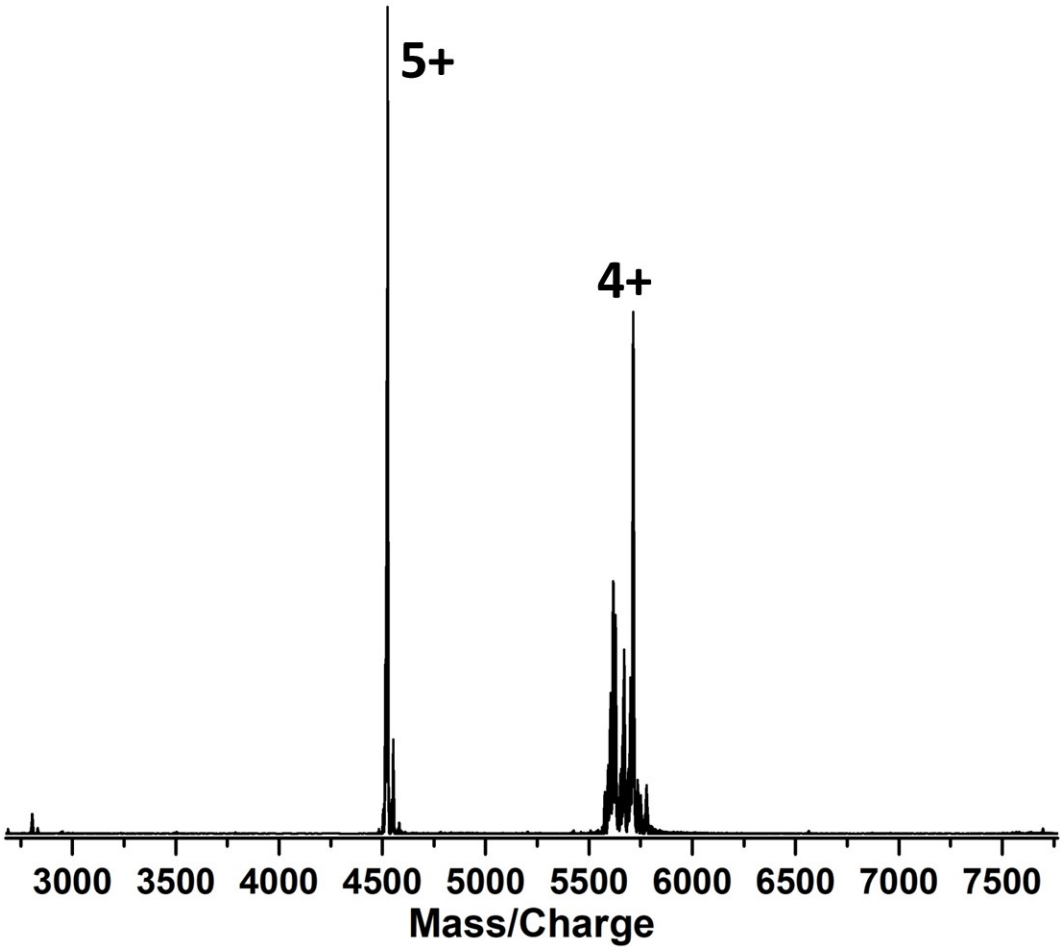

Figure S21. Positive-ion mode ESI-MS of Ag_{148}.

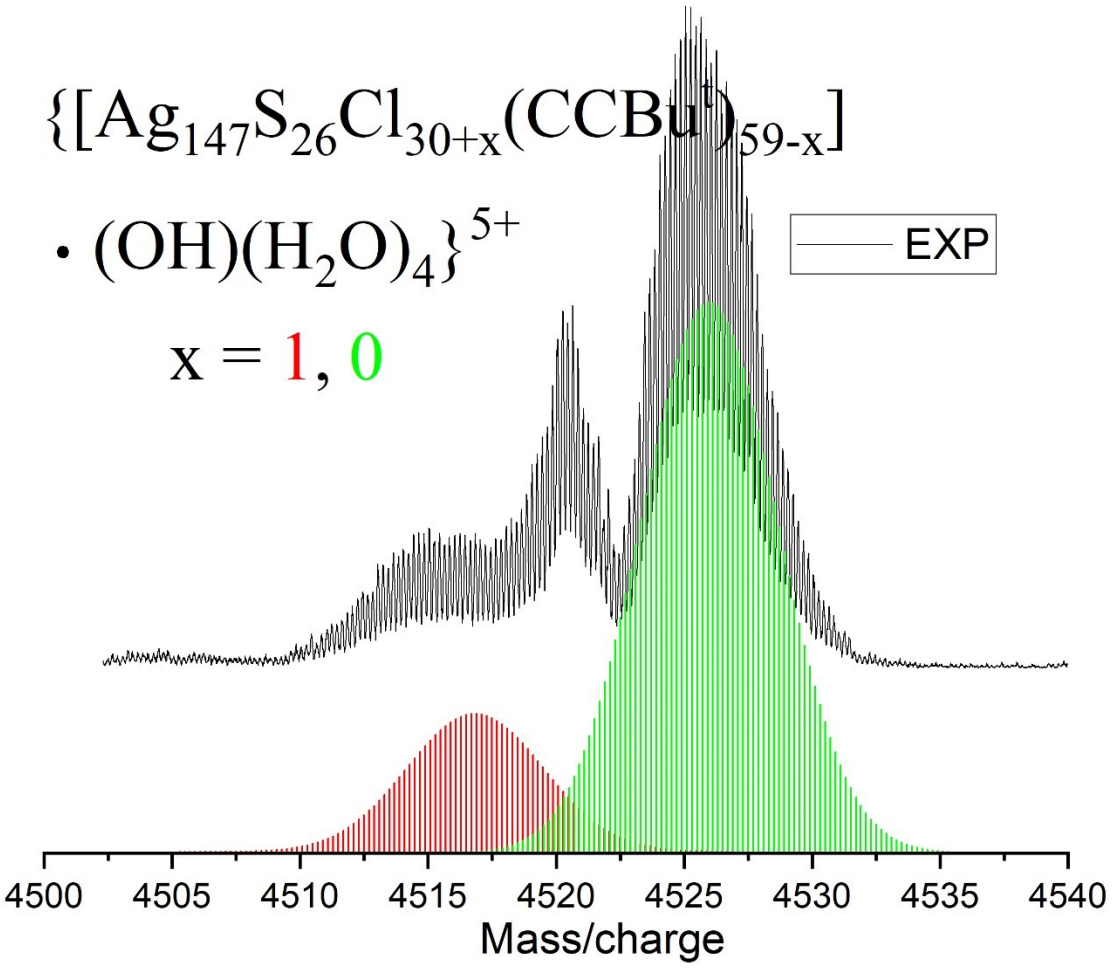

Figure S22. Experimental (black) and simulated mass spectrometry (multicolor).

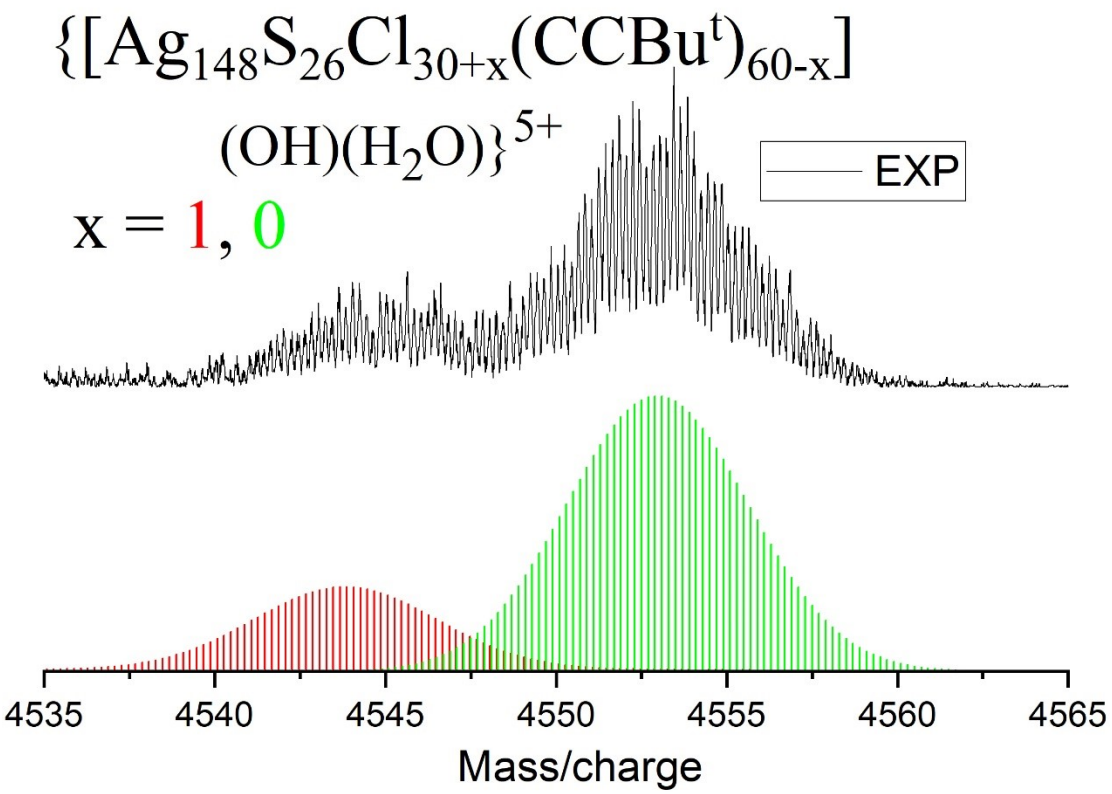

Figure S23. Experimental (black) and simulated mass spectrometry (multicolor).

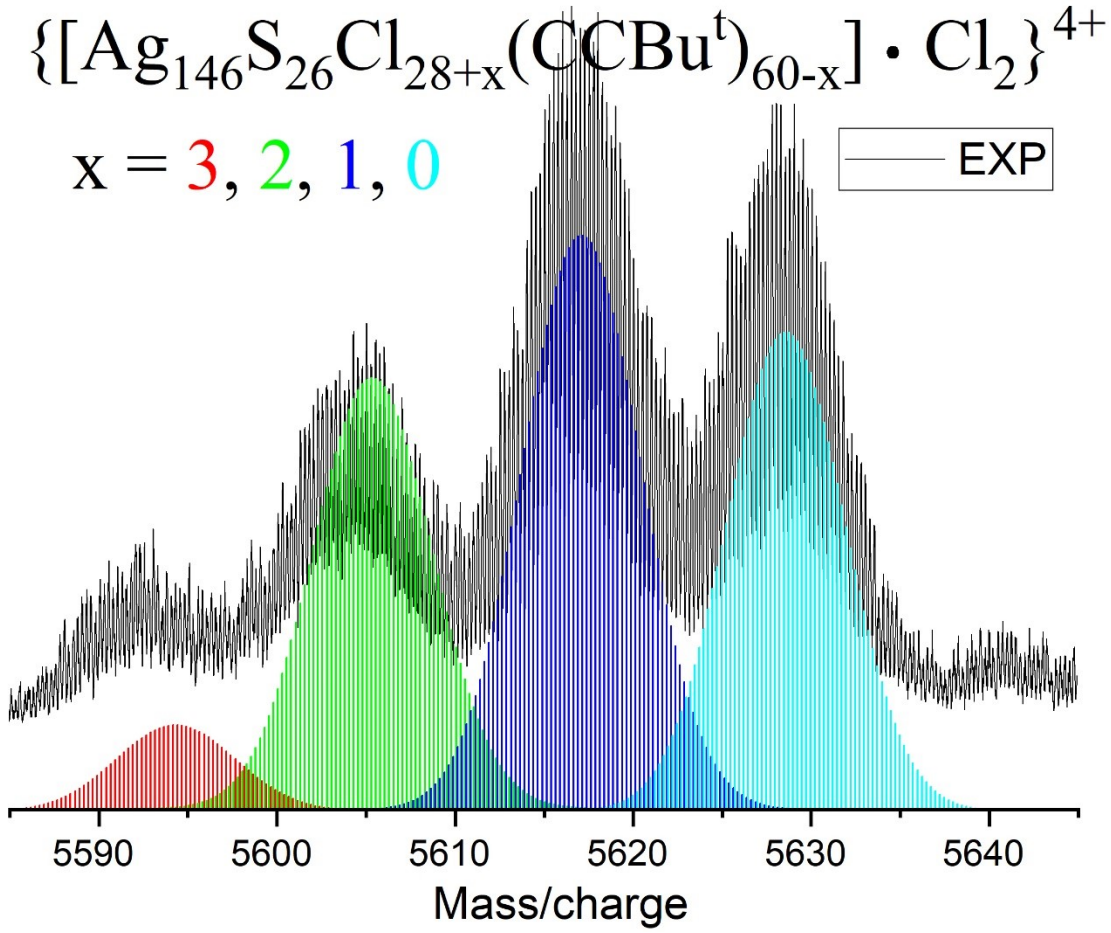

Figure S24. Experimental (black) and simulated mass spectrometry (multicolor)..

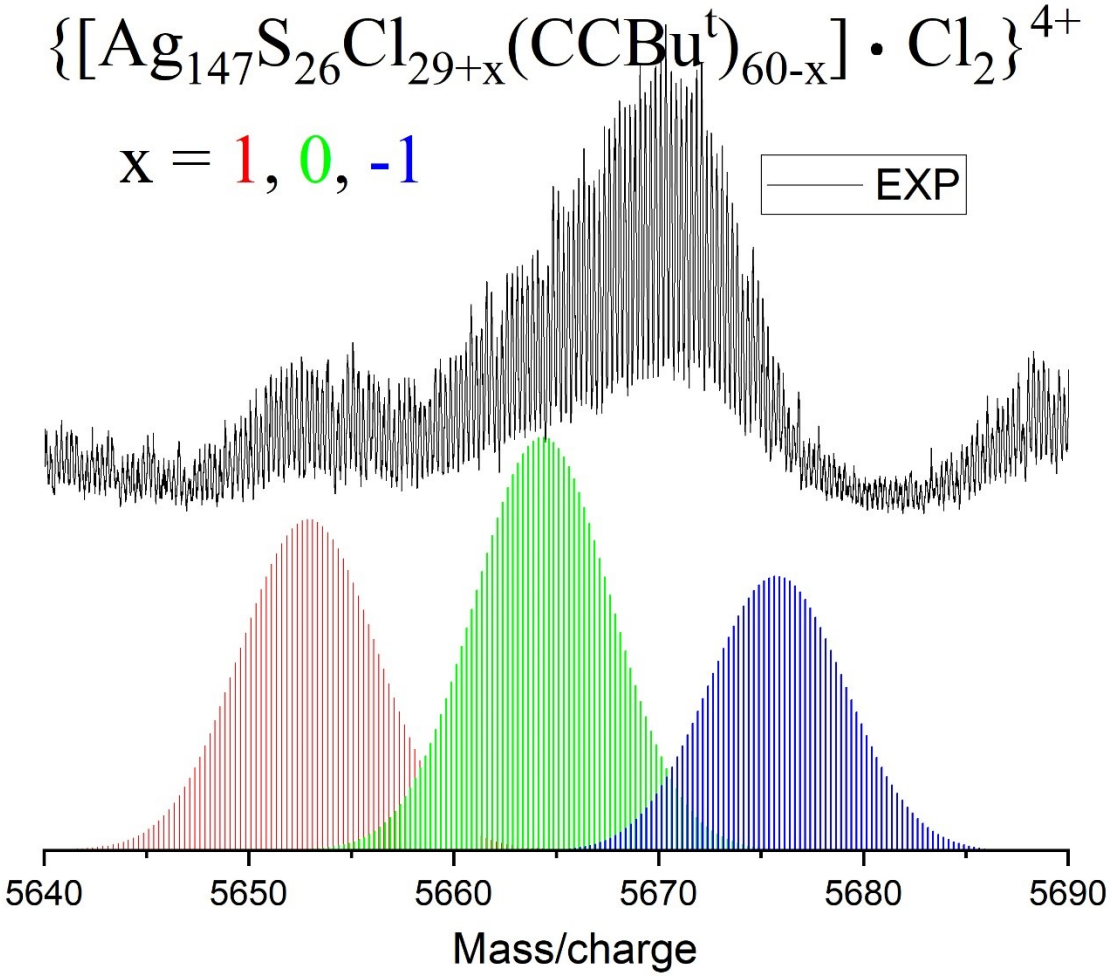

Figure S25. Experimental (black) and simulated mass spectrometry (multicolor).

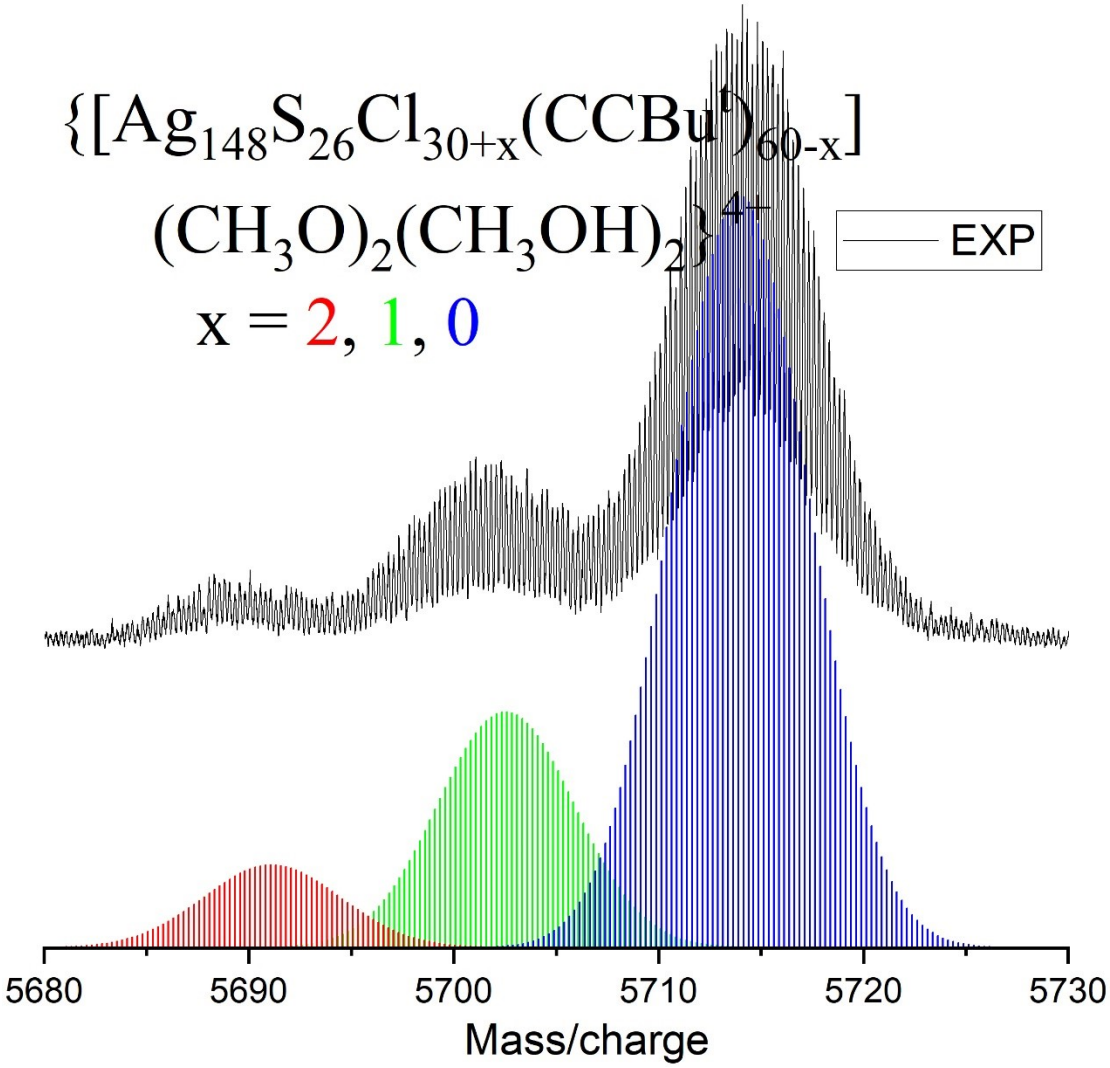

Figure S26. Experimental (black) and simulated mass spectrometry (multicolor).

Table S4. Assignment of the highest +5 and +4 species of Ag_{148} identified by ESI-MS.

$[Ag_{148}S_{26}Cl_{30}(C_6H_9)_{60}]^{6+}$ represent intact cation of cluster, C_6H_9 represent $(CCBu^t)^-$.

The strongest +5 peak of exp.	4525.67
assignment	Cal.
$\{[Ag_{148}S_{26}Cl_{30}(C_6H_9)_{60}]^{6+}\text{-}Ag_1\}^{5+}$	4524.31
$\{[Ag_{148}S_{26}Cl_{30}(C_6H_9)_{60}]^{6+}\text{-}Ag_1\}^{5+}H_2O$	4527.92
$\{[Ag_{148}S_{26}Cl_{30}(C_6H_9)_{60}]^{6+}\text{-}AgCl+(CH_3O)_1\}^{5+}$	4523.52
$\{[Ag_{148}S_{26}Cl_{30}(C_6H_9)_{60}]^{6+}\text{-}AgCl+(CH_3O)_1(H_2O)_1\}^{5+}$	4527.13
$\{[Ag_{148}S_{26}Cl_{30}(C_6H_9)_{60}]^{6+}\text{-}AgCl+(OH)_1(H_2O)_1\}^{5+}$	4524.32
$\{[Ag_{148}S_{26}Cl_{30}(C_6H_9)_{60}]^{6+}\text{-}AgCl+Cl\}^{5+}$	4524.31
$\{[Ag_{148}S_{26}Cl_{30}(C_6H_9)_{60}]^{6+}\text{-}AgCl+(Cl)_1(H_2O)_1\}^{5+}$	4527.92
$\{[Ag_{148}S_{26}Cl_{30}(C_6H_9)_{60}]^{6+}\text{-}AgC_6H_9+(Cl)_1(H_2O)_3\}^{5+}$	4526.10
$\{[Ag_{148}S_{26}Cl_{30}(C_6H_9)_{60}]^{6+}\text{-}AgC_6H_9+(Cl)_1(H_2O)_1(CH_3OH)_1\}^{5+}$	4525.30
$\{[Ag_{148}S_{26}Cl_{30}(C_6H_9)_{60}]^{6+}\text{-}AgC_6H_9+(CH_3O)_1(CH_3OH)_2\}^{5+}$	4527.11
$\{[Ag_{148}S_{26}Cl_{30}(C_6H_9)_{60}]^{6+}\text{-}AgC_6H_9+(OH)_1(CH_3OH)_2\}^{5+}$	4524.31
$\{[Ag_{148}S_{26}Cl_{30}(C_6H_9)_{60}]^{6+}\text{-}AgC_6H_9+(OH)_1(H_2O)_4\}^{5+}$	4525.91
$\{[Ag_{148}S_{26}Cl_{30}(C_6H_9)_{60}]^{6+}+Cl_1\}^{5+}$	4553.09
$\{[Ag_{148}S_{26}Cl_{30}(C_6H_9)_{60}]^{6+}+(OH)_1\}^{5+}$	4549.30
$\{[Ag_{148}S_{26}Cl_{30}(C_6H_9)_{60}]^{6+}+(CH_3O)_1\}^{5+}$	4552.10

The strongest +4 peak of exp.	5714.08
assignment	Cal.
$\{[Ag_{148}S_{26}Cl_{30}(C_6H_9)_{60}]^{6+}Cl_2\}^{4+}$	5700.10
$\{[Ag_{148}S_{26}Cl_{30}(C_6H_9)_{60}]^{6+}Cl_2(H_2O)_2\}^{4+}$	5709.11
$\{[Ag_{148}S_{26}Cl_{30}(C_6H_9)_{60}]^{6+}Cl_2(CH_3OH)_2\}^{4+}$	5716.12
$\{[Ag_{148}S_{26}Cl_{30}(C_6H_9)_{60}]^{6+}Cl_2(CH_3CN)_2\}^{4+}$	5720.62
$\{[Ag_{148}S_{26}Cl_{30}(C_6H_9)_{60}]^{6+}Cl_2(CH_2Cl_2)_1\}^{4+}$	5721.34
$\{[Ag_{148}S_{26}Cl_{30}(C_6H_9)_{60}]^{6+}Cl_2(CH_3CN)_1\}^{4+}$	5710.36
$\{[Ag_{148}S_{26}Cl_{30}(C_6H_9)_{60}]^{6+}Cl_2(CH_3COCH_3)_1\}^{4+}$	5714.61
$\{[Ag_{148}S_{26}Cl_{30}(C_6H_9)_{60}]^{6+}Cl_2(H_2O)_1(CH_3CN)_1\}^{4+}$	5714.86
$\{[Ag_{148}S_{26}Cl_{30}(C_6H_9)_{60}]^{6+}Cl_2(H_2O)_1(CH_3OH)_1\}^{4+}$	5712.61
$\{[Ag_{148}S_{26}Cl_{30}(C_6H_9)_{60}]^{6+}Cl_1(C_6H_9)_1\}^{4+}$	5711.63
$\{[Ag_{148}S_{26}Cl_{30}(C_6H_9)_{60}]^{6+}Cl_1(C_6H_9)_1(H_2O)_1\}^{4+}$	5716.13
$\{[Ag_{148}S_{26}Cl_{30}(C_6H_9)_{60}]^{6+}(OH)_2\}^{4+}$	5690.87
$\{[Ag_{148}S_{26}Cl_{30}(C_6H_9)_{60}]^{6+}(OH)_2(H_2O)_5\}^{4+}$	5713.38
$\{[Ag_{148}S_{26}Cl_{30}(C_6H_9)_{60}]^{6+}(OH)_2(CH_3OH)_3\}^{4+}$	5714.89
$\{[Ag_{148}S_{26}Cl_{30}(C_6H_9)_{60}]^{6+}(OH)_2(CH_3CN)_2\}^{4+}$	5711.38
$\{[Ag_{148}S_{26}Cl_{30}(C_6H_9)_{60}]^{6+}(OH)_2(CH_3COCH_3)_2\}^{4+}$	5719.89
$\{[Ag_{148}S_{26}Cl_{30}(C_6H_9)_{60}]^{6+}(OH)_2(CH_2Cl_2\}^{4+}$	5712.11
$\{[Ag_{148}S_{26}Cl_{30}(C_6H_9)_{60}]^{6+}(OH)_1Cl_1\}^{4+}$	5695.61
$\{[Ag_{148}S_{26}Cl_{30}(C_6H_9)_{60}]^{6+}(OH)_1Cl_1(H_2O)_4\}^{4+}$	5713.62
$\{[Ag_{148}S_{26}Cl_{30}(C_6H_9)_{60}]^{6+}(OH)_1Cl_1(CH_3OH)_2\}^{4+}$	5711.63
$\{[Ag_{148}S_{26}Cl_{30}(C_6H_9)_{60}]^{6+}(OH)_1Cl_1(CH_3CN)_2\}^{4+}$	5716.13
$\{[Ag_{148}S_{26}Cl_{30}(C_6H_9)_{60}]^{6+}(OH)_1Cl_1(CH_2Cl_2)_1\}^{4+}$	5716.60
$\{[Ag_{148}S_{26}Cl_{30}(C_6H_9)_{60}]^{6+}(OH)_1Cl_1(CH_3COCH_3)_1\}^{4+}$	5710.12
$\{[Ag_{148}S_{26}Cl_{30}(C_6H_9)_{60}]^{6+}(CH_3O)_2\}^{4+}$	5697.88
$\{[Ag_{148}S_{26}Cl_{30}(C_6H_9)_{60}]^{6+}(CH_3O)_2(CH_3OH)_2\}^{4+}$	5713.89
$\{[Ag_{148}S_{26}Cl_{30}(C_6H_9)_{60}]^{6+}(CH_3O)_2(CH_3CN)_2\}^{4+}$	5718.39
$\{[Ag_{148}S_{26}Cl_{30}(C_6H_9)_{60}]^{6+}(CH_3O)_2(CH_3COCH_3)_1\}^{4+}$	5712.39
$\{[Ag_{148}S_{26}Cl_{30}(C_6H_9)_{60}]^{6+}(CH_3O)_2(CH_2Cl_2)_1\}^{4+}$	5719.12
$\{[Ag_{148}S_{26}Cl_{30}(C_6H_9)_{60}]^{6+}(CH_3O)_2(H_2O)_4\}^{4+}$	5715.89
$\{[Ag_{148}S_{26}Cl_{30}(C_6H_9)_{60}]^{6+}(CH_3O)_1Cl_1(CH_3OH)_2\}^{4+}$	5715.13
$\{[Ag_{148}S_{26}Cl_{30}(C_6H_9)_{60}]^{6+}(CH_3O)_1Cl_1(CH_3COCH_3)_1\}^{4+}$	5713.63
$\{[Ag_{148}S_{26}Cl_{30}(C_6H_9)_{60}]^{6+}(CH_3O)_1(OH)_1(CH_3OH)_2\}^{4+}$	5710.39
$\{[Ag_{148}S_{26}Cl_{30}(C_6H_9)_{60}]^{6+}(CH_3O)_1(OH)_1(CH_3OH)_2(H_2O)_1\}^{4+}$	5714.89

The comparison to the solid state Ag_2S and AgCl structure with Ag_{148}

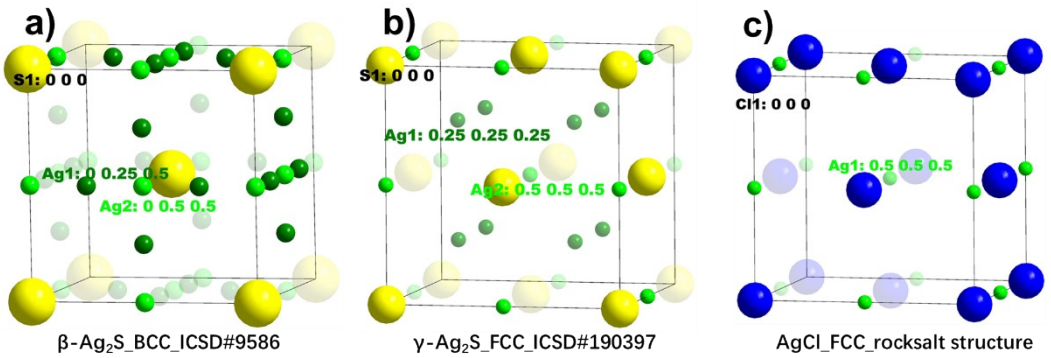

Figure S27. (a) Interstices of S framework (BCC) occupied by Ag atoms, tetrahedral void green Ag, octahedral void bright green Ag; (b) Interstices of S framework (FCC) occupied by Ag atoms, tetrahedral void green Ag, octahedral void bright green Ag; (c) Interstices of Cl framework (FCC) occupied by Ag atoms, octahedral void bright green Ag.

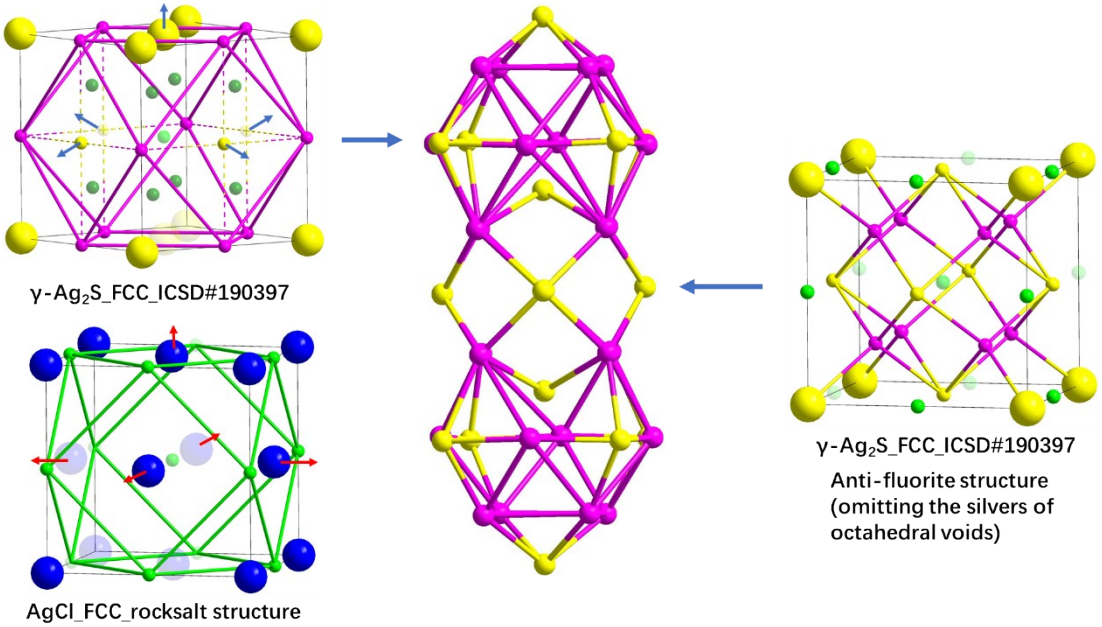

Figure S28. The comparison to the solid state Ag_2S and AgCl structure with $Ag_{24}X_{16}$.

The central Ag_8X_6 can be a fragment of anti-fluorite structure, the two-side $Ag_{12}X_5$ can be a fragment of solid state Ag_2S or AgCl considering the movement of anions.

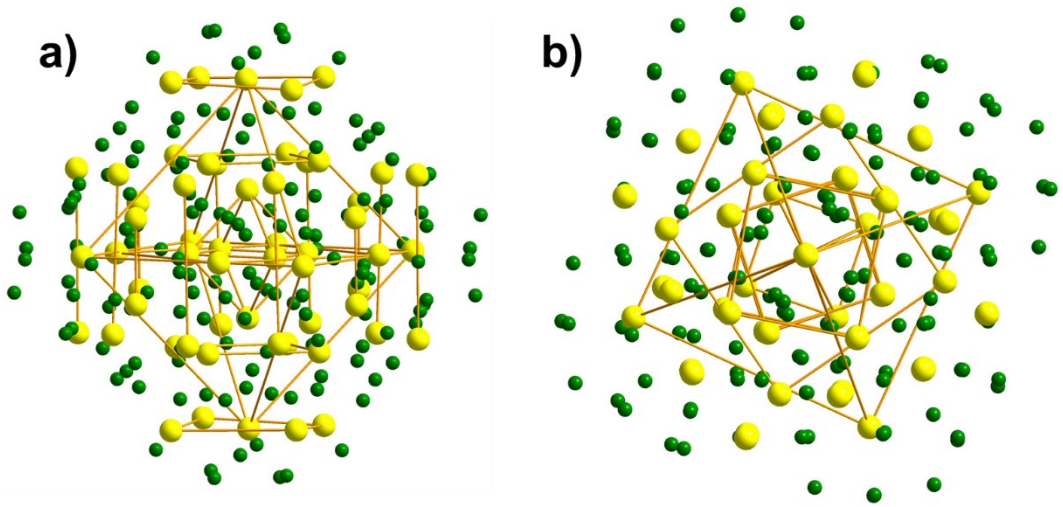

Figure S29. The sites of X and Ag atoms of Ag_{148}, side and top view.

Although there are some rules in the distribution of anions, it does not conform to the highly symmetrical face-centered cubic or body-centered cubic arrangement as a whole.

Ag-Ag and Ag-X bond lengths in Ag_{148}

Table S5. A summary of Ag-Ag and Ag-X bond lengths in Ag_{148}.

Entry	Ag-Ag distance	average value	Ag-X distance	average value
Shell 1	2.899~3.354 Å	3.126 Å	2.469~2.732 Å	2.601 Å
1st and 2nd	2.905~3.283 Å	3.094 Å	2.393~3.103 Å	2.748 Å
Shell 2	2.835~3.619 Å	3.227 Å	2.327~3.146 Å	2.736 Å
2nd and 3rd	2.892~3.676 Å	3.284 Å	2.359~3.400 Å	2.879 Å
Shell 3	2.848~3.604 Å	3.226 Å	2.639~3.099 Å	2.883 Å

Connection between different shell layers

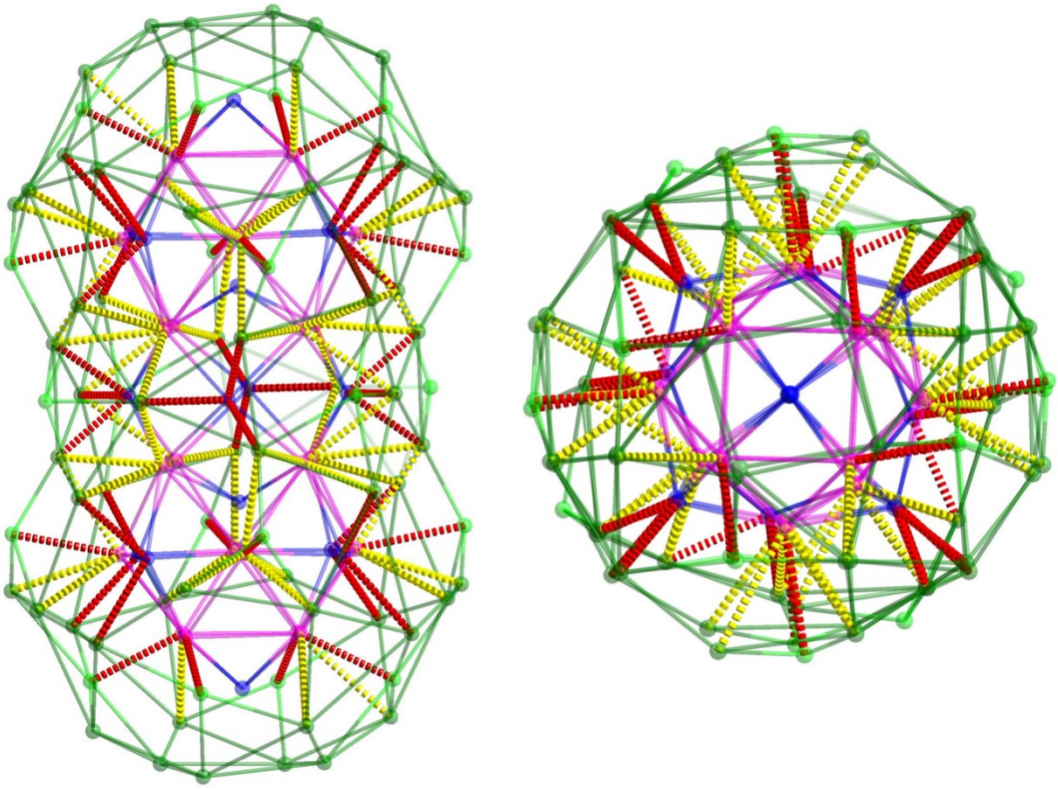

Figure S30. The $Ag_{24}X_{16}$ peanut kernel and the $Ag_{60}X_{20}$ shell are linked by Ag-Ag interaction (yellow dotted line) and Ag-X interaction (red dotted line).

Four X of rhombohedral Ag_8X_6 connect four Ag_3 triangles of $Ag_{60}X_{20}$ shell at the waist. Eight X capped on cuboctahedron bond to one Ag of inner cubocatahedron Ag_{24}. Ag–Ag and Ag–X bond lengths are listed in Table S5.

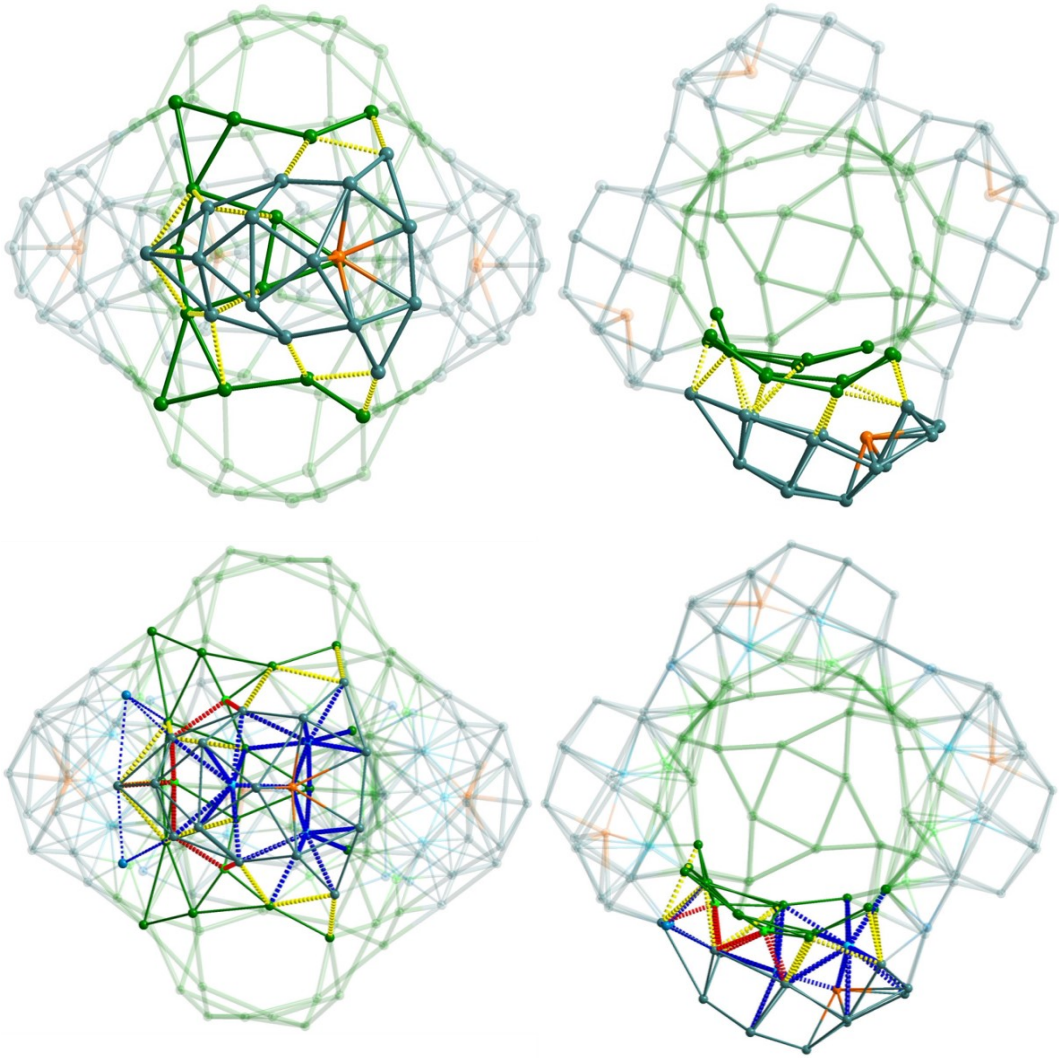

Figure S31. The interaction of Ag-Ag (yellow dotted line) and Ag-X (red and blue dotted line) between the windmill-like shell and the peanut-shaped shell

The head of Ag_{16} boat above the inner Ag_5 pentagon is stabilized by three X of peanut shell, and the tail of Ag_{16} boat is connected to each side of the two inner Ag_6 hexagons. X of X_3Ag tetrahedron not only firmly grasps the Ag at the apex of the concave body, but also further stabilizes the peanut shell and the outermost windmill shell. A summary of Ag–Ag and Ag–X distances is presented in Table S5.

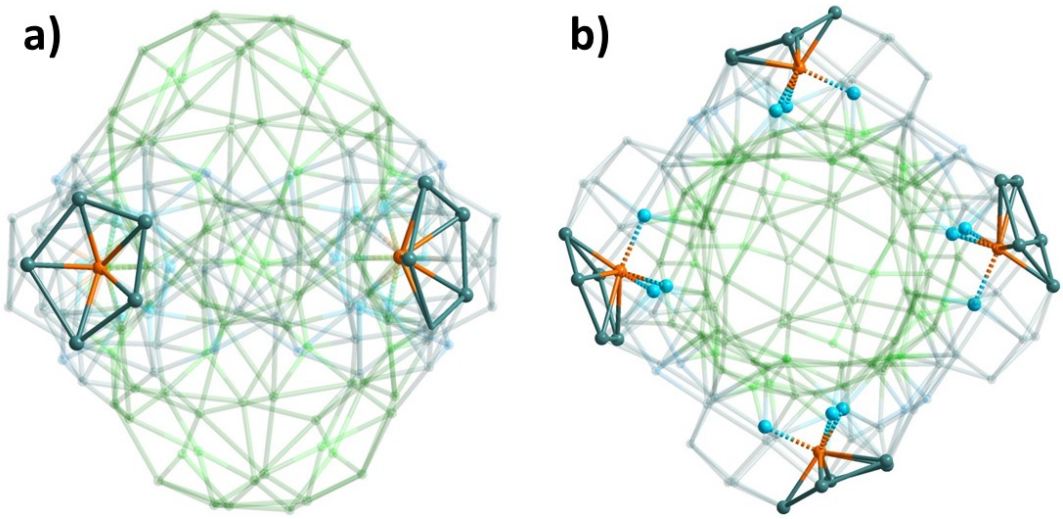

Figure S32. Side and top views of Ag_6 concave polyhedron with vertex Ag in orange strengthened by three sky blue anions.

Table S6: A list of reported core-shell structured silver sulfide clusters with crystal structures.

Cluster composition	Core-shell	Shell count	Ref.
$Ag_{45}S_6(C{\equiv}C^tBu)_{32}^-$	$Ag_1@Ag_8@Ag_{36}$	3	4
$[Ag_{216}S_{56}C_{17}(C{\equiv}CPh)_{98}]^-$	$Ag_{12}@Ag_{36}@Ag_{172}$	3	5
$[Ag_{73}S_{14}(^tBuS)_{32}(PPA)_{12}]^{11-}$	$Ag_1@Ag_{24}@Ag_{48}$	3	6
$Ag_{66}S_6(^tBuS)_{24}(PPA)_{12}(HPPA)_2(CN)_4$	$Ag_{20}@Ag_{44}$	2	6
$Ag_{78}S_{13}(^tBuS)_{28}(MeOPhCOO)_{14}(MoO_4)_5{\cdot}CH_3CN$	$Ag_{21}@Ag_{57}$	2	7
$Ag_{56}S_{12}(S^tBu)_{20}(Sal)_{12}$	$Ag_{14}@Ag_{42}$	2	8
$Ag_{56}S_{13}(S^tBu)_{20}]^{10+}$	$Ag_{14}@Ag_{42}$	2	9
$Ag_{48}S(^tBuS)_{23}(^nBuPO_3)_9(CH_3O)_2(NO)_3{\cdot}2CH_3OH$	$Ag_{12}@Ag_{36}$	2	10
$(MoO_4)_2Ag_{51}S(^tBuS)_{27}(^nBuPO_3)_7(CH_3O)_2(NO_3)_2$	$Ag_{11}@Ag_{40}$	2	10
$[MoO_4Ag_{48}S_6(^tBuS)_{24}(^nBuP03)_8]^{6+}$	$Ag_{12}@Ag_{36}$	2	10
$[Ag_{62}S_{13}(SBut)_{32}]^{4+}$	$Ag_{14}@Ag_{45}$	2	11
$[Ag_{60}S_{15}(iPrS)_{24}(CF_3SO_3)_{14}(CH_3OH)_4(DMF)_2]^{8+}$	$Ag_{12}@Ag_{48}$	2	12
$[SO_4Ag_{78}S_{15}(CpS)_{27}(CF_3CO2)_{12}]^{7+}$	$Ag_{18}@Ag_{60}$	2	13
$Ag_{48}S_7(^tBuC{\equiv}C)_{12}(^tBuS)_{12}(^nBuPO_3)_2(^nBuPO_3H)_6$	$Ag_{12}@Ag_{36}$	2	14
$[Ag_{33}S_3(^tBuC{\equiv}C)_{12}(^tBuS)_{18}(^nBuPO_3)(^nBuPO_3H)(NO_3)_4]^{4-}$	$Ag_3@Ag_{42}$	2	14
$Ag_{45}S_6(^tBuC{\equiv}C)_6(^tBuS)_{12}(^tBuPO_3)(^tBuPO_3H)(hfac)_6$	$Ag_3@Ag_{30}$	2	14
$(PO4)_8Ag_{90}S_6(^tBuS)_{24}(PhPO_3)_{12}(PhPO_3H)_6$	$Ag_6@Ag_{24}@Ag_{60}$	3	15
$Ag_{102}S_6(PO_4)_8((CyS)_{30}(H_2PO_4)_6(HPO_4)_6(CF_3COO)_{18})$	$Ag_6@Ag_{24}@Ag_{60}@Ag_{12}$	4	16
$(SO_4)_{36}S_{22}Ag_{192}(CyhS)_{66}(NO_3)_{12}$	$Ag_6@Ag_{24}@Ag_{12}@Ag_6@Ag_{12}@Ag_{132}$	6	17
$[Ag_{148}S_{26}Cl_{30}(Bu^tC{\equiv}C)_{60}]^{6+}$	$Ag_{24}@Ag_{60}@Ag_{64}$	3	This work

TEM image of Ag_{148}

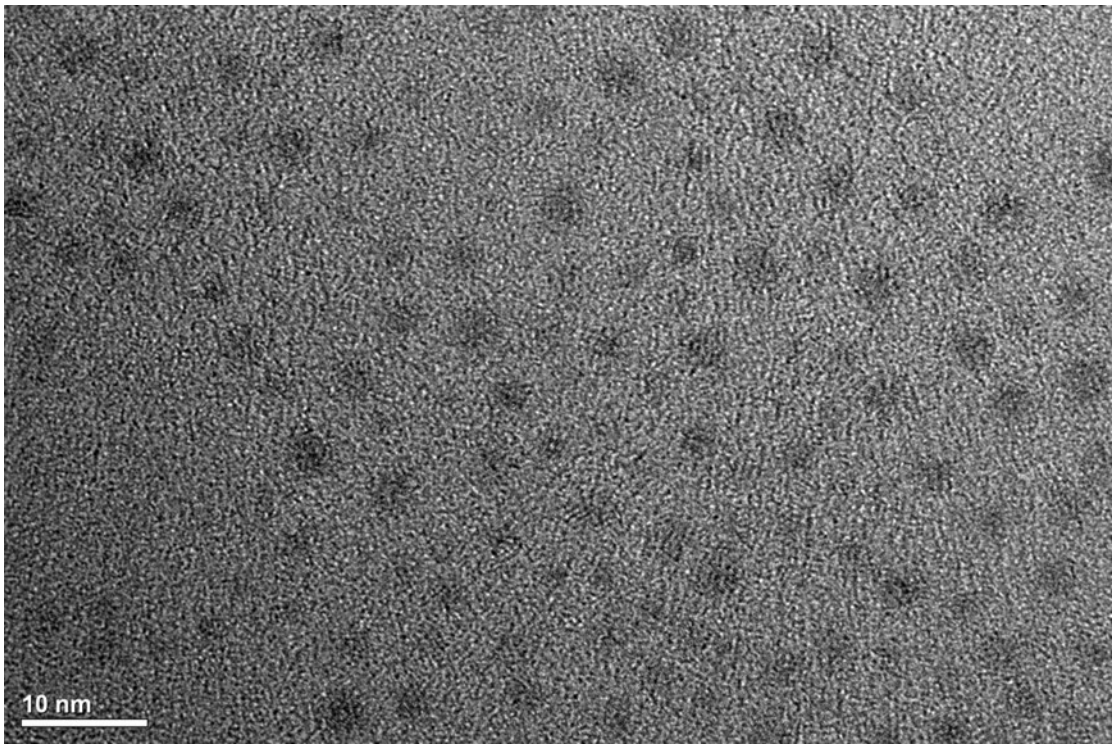

Figure S33. TEM image of Ag_{148} dissolved in dichloromethane

Coordination modes of alkynyl ligands

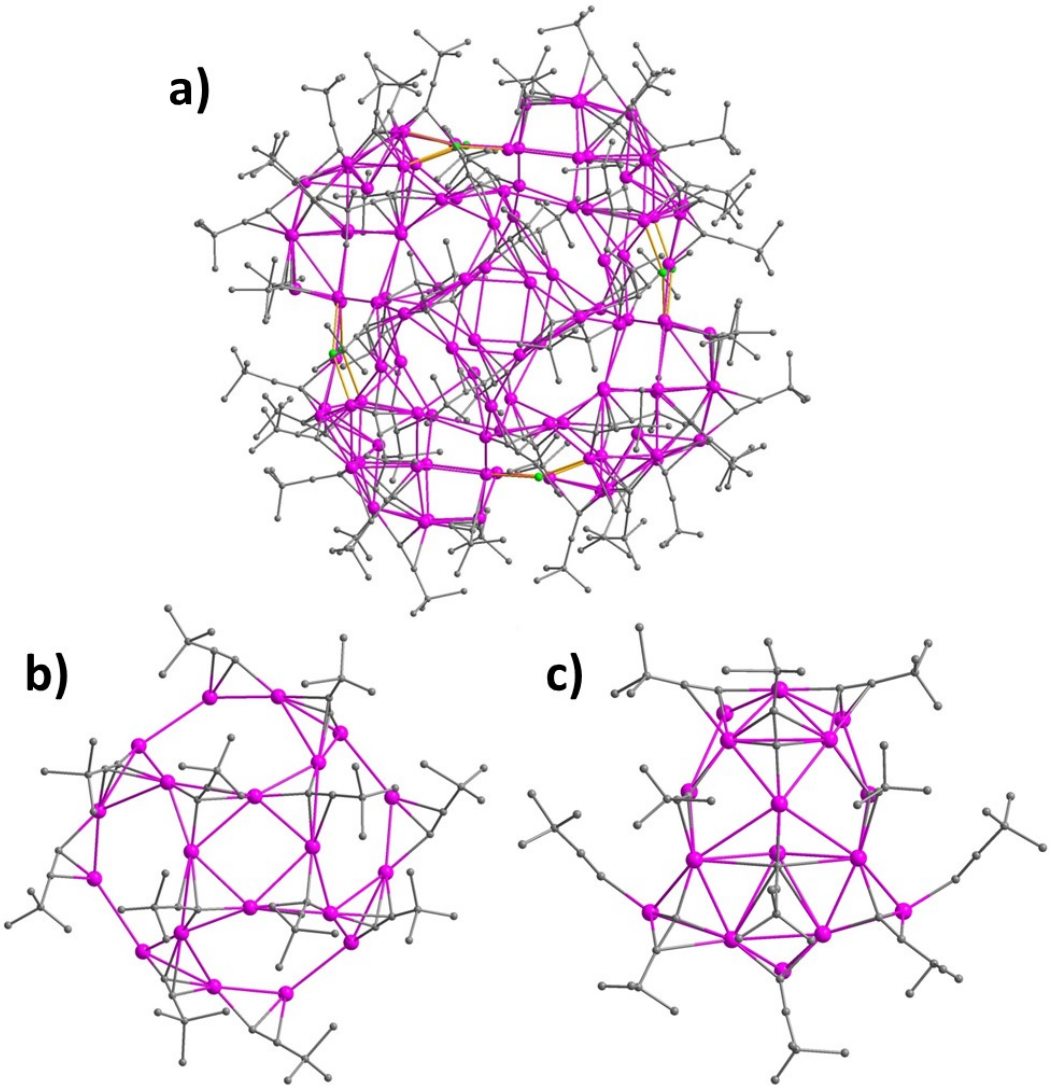

Figure S34. Coordination modes of alkynyl ligands connected with Ag atoms. Color codes: pink, Ag; dark grey, C.

The distribution and template motifs of 56 X anions in Ag_{148}

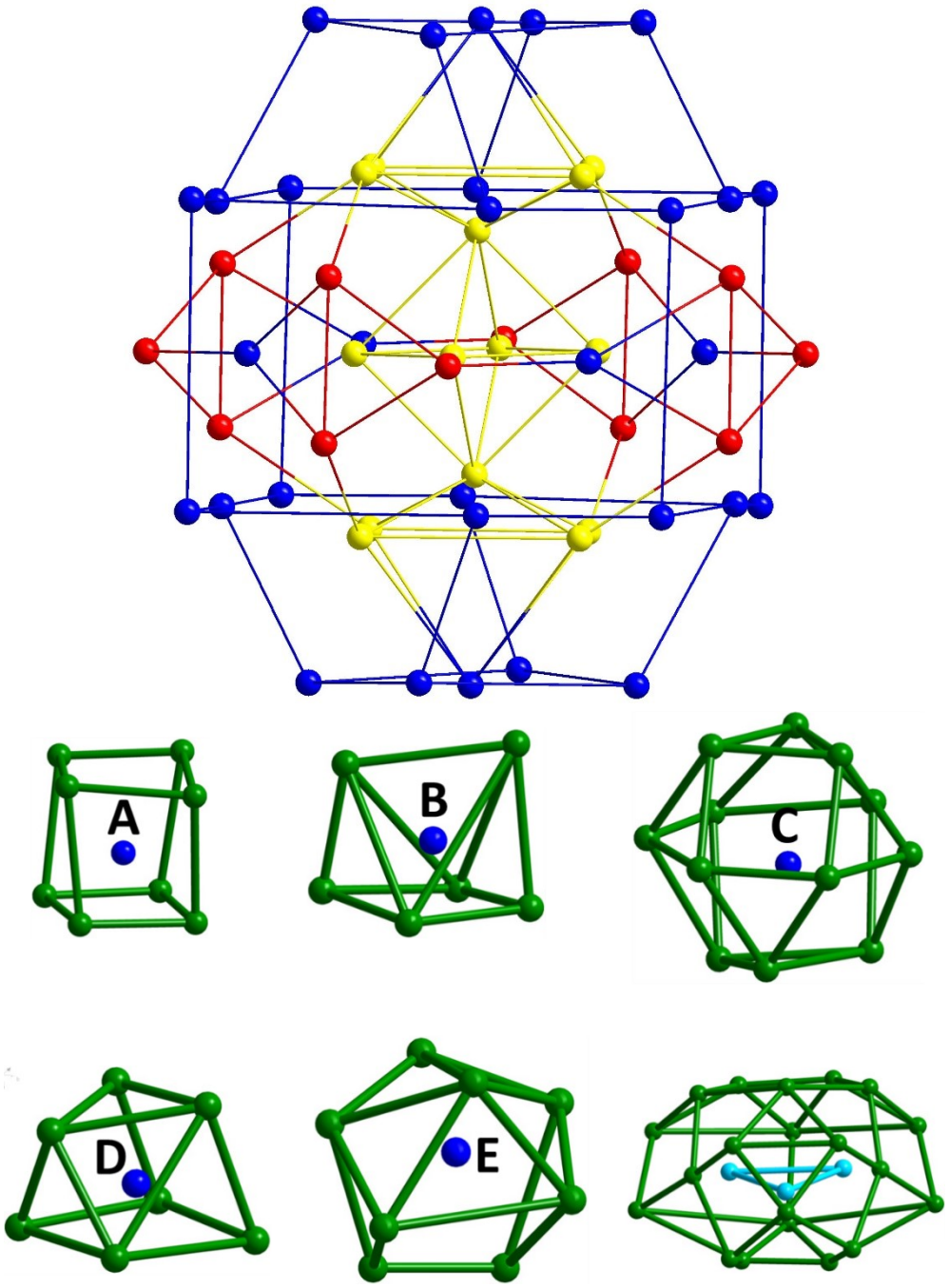

Figure S35. The distribution of 56 X anions, blue yellow and red represent X (top); six template motifs (down).

Time-dependent UV−vis of Ag_{148}

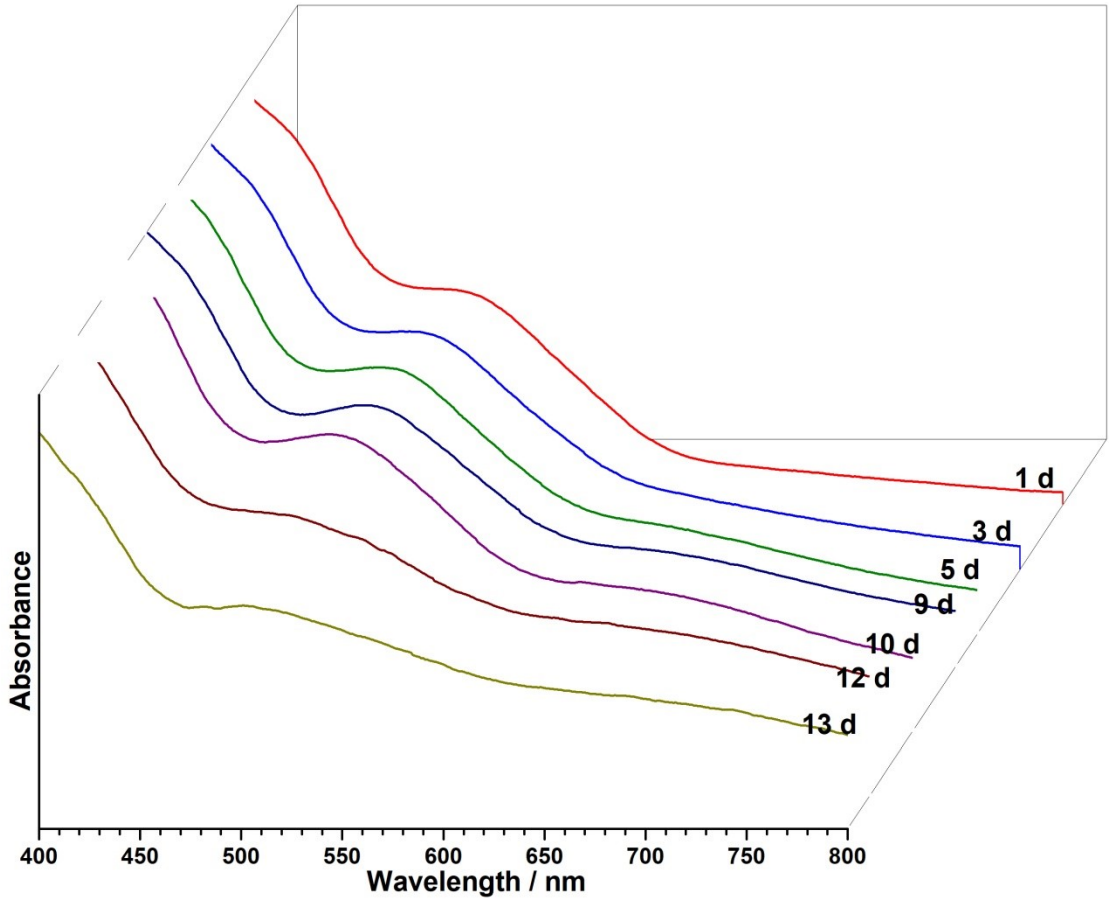

Figure S36. Time-dependent UV−vis absorption spectrum of Ag_{148} in CH_2C_{l2} under ambient conditions.

The quantum yield of Ag_{148} compared to RhB

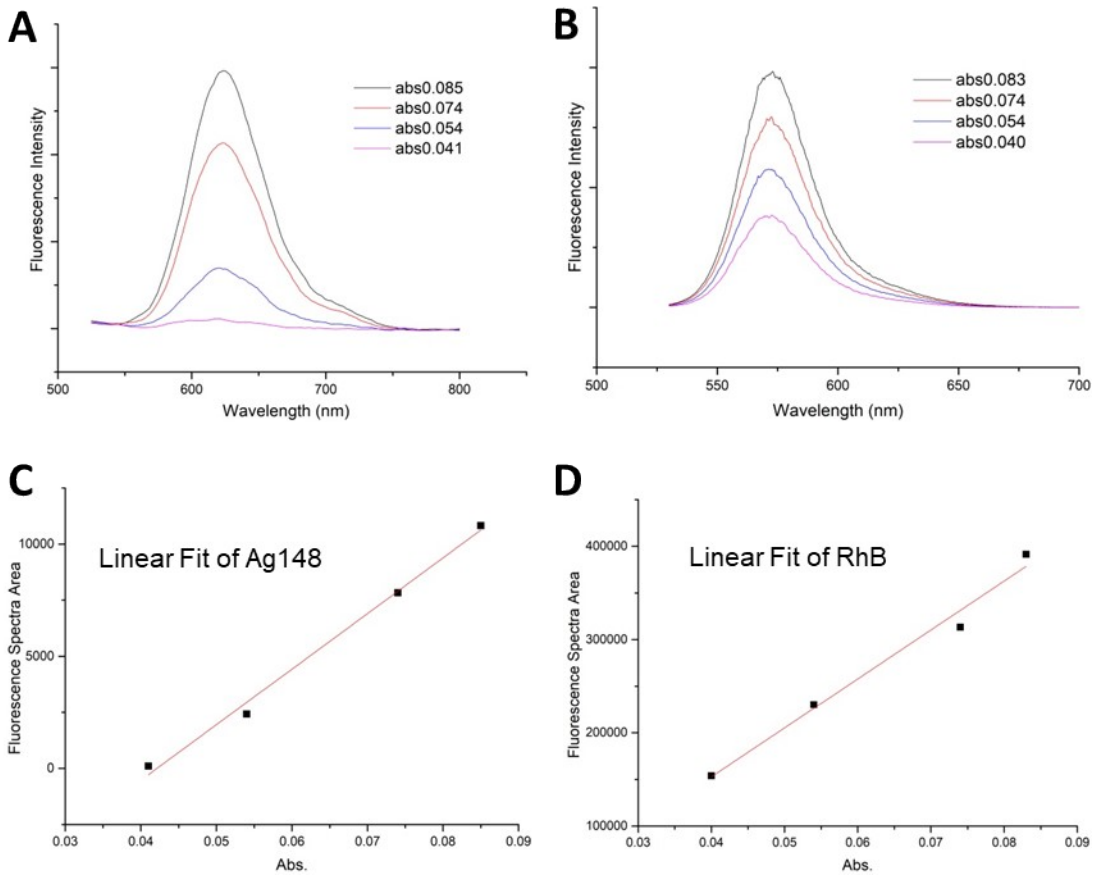

Figure S37. (A) Fluorescence spectra of the Ag_{148} nanocluster with different absorbance (in CH_2Cl_2 solution). (B) Fluorescence spectra of Rhodamine B with different absorbance (in CH3CH2OH solution). (C) Absorbance vs. area of fluorescence of the Ag_{148} nanocluster. (D) Absorbance vs. area of fluorescence of Rhodamine B. The quantum yield (QY) of the Ag_{148} nanocluster can be calculated using the formula of: $QY(Ag_{148}) = QY(RhB) * (Grad_{cluster}/Grad_{RhB}) * [(n_{CH2Cl2})^2/(n_{CH3CH2OH})^2]$, wherein QY(RhB) is 69%; $Grad_{cluster}$ and $Grad_{RhB}$ are 2477740 and 5249060, respectively; n is the refractive index of the solvent, and n_{CH2Cl2} and $n_{CH3CH2OH}$ are 1.4241 and 1.3614, respectively. In this context, the PL QY of Ag_{148} nanocluster is 39.6%.

Emission decay of Ag_{148}

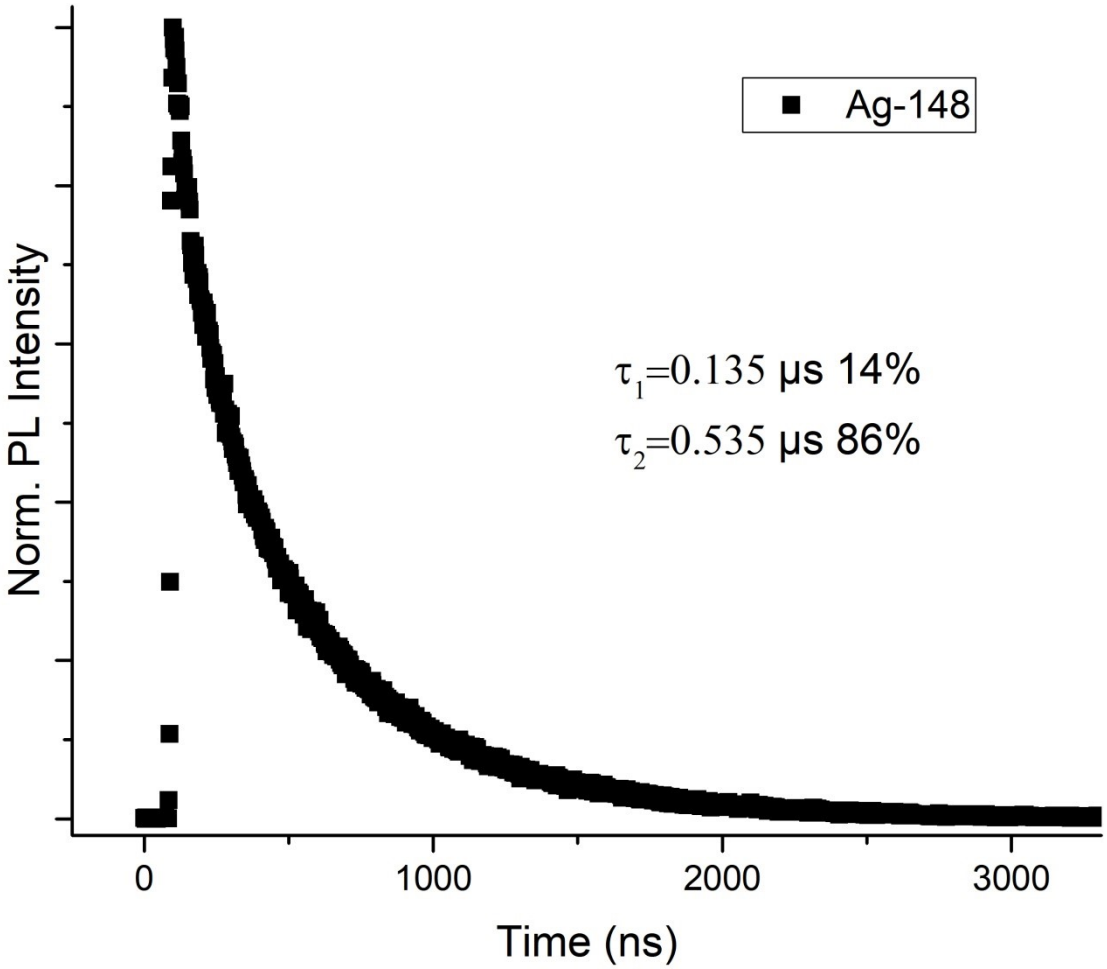

Figure S38. The TRPL data for Ag_{148}. The kinetic traces could be fitted with bi-exponential equations with corresponding lifetimes of 0.135 μs (14 %) and 0.535 μs (86%).

Time-dependent EM of Ag_{148}

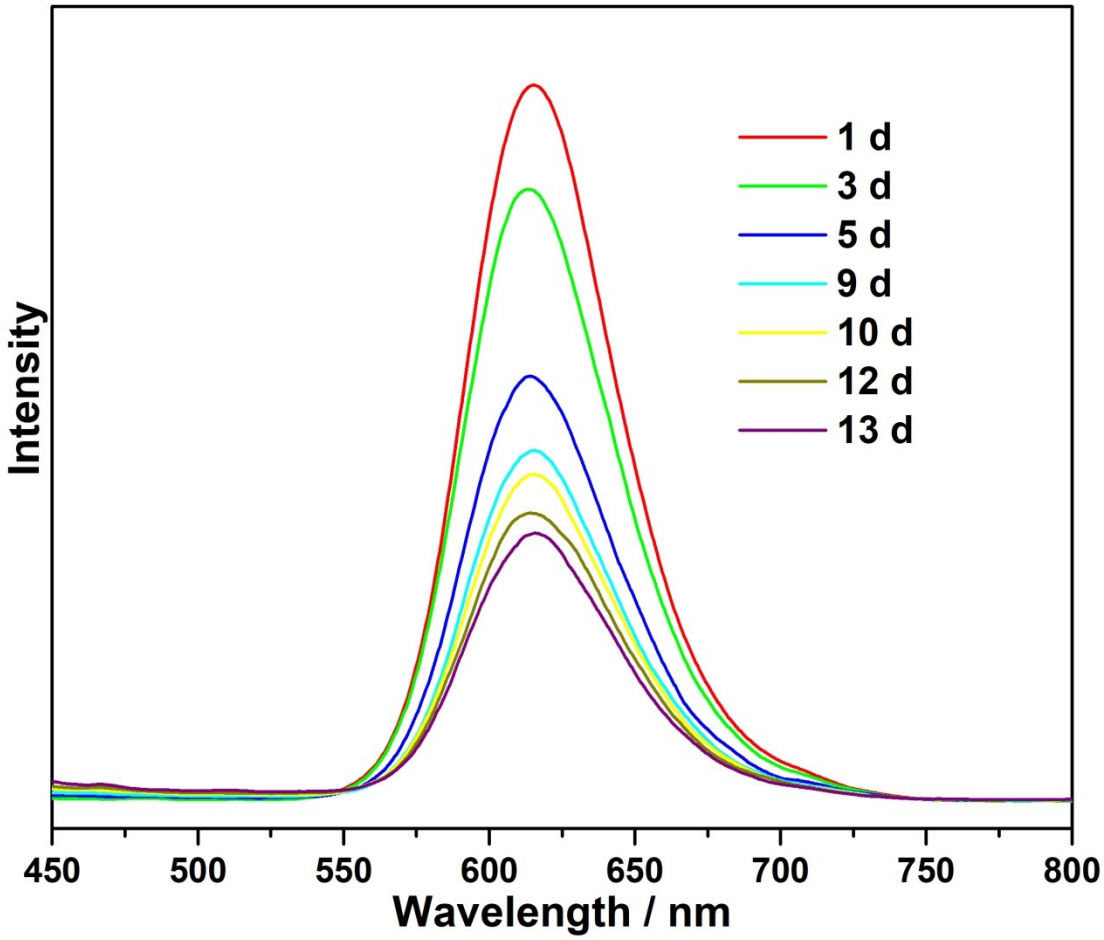

Figure S39. Time-dependent emission spectra of Ag_{148} in CH_2Cl_2 under ambient conditions.

The biomedical applications of Ag_{148}

Cell culture.

Human colorectal cancer cell (SW620), lung adenocarcinoma (A549), and cervical cancer cell (Hela) were grown in high-glucose Dulbecco's modified Eagle's medium (DMEM, HyClone) with supplements of 10% (v/v) fetal bovine serum (PAN) and 1% penicillin/streptomycin(Gibico) at 37 °C with 5% CO2.

Absorption identification of Ag_{148}

Dissolve 10 mg Ag_{148} in 1mL DMSO and dilute the material at the ratio of 0.1,1,4,10 ug/ml. In order to study the absorption of the material, the confocal microscope was used to observe the absorption of the material at 6h and 9h after adding the material.

MTT assay.

Cells were seeded in 96-well plates (1 $x10^3$ cells per well) and cultivated at 37 ℃ in a 5% CO_2 humidified incubator for 24 h. After 0.1,1,4,10ug/ml Ag_{148} were added to the medium and incubated for 12 h, 20 μl of MTT solution (MTT, Sigma-Aldrich) were added to each well, followed by 4 h of incubation at 37 ℃. After the medium was removed, 150 μL Dimethyl sulfoxide (DMSO) was added and the optical density (OD) at 490 nm was measured using a Spectrometer Varioskan Flash (ThermoFisher). A proliferation curve was drawn with the time as the abscissa and the average absorbance value in each group as the ordinate. Triplicate reactions were performed for the experiment.

Apoptosis analysis.

For cell apoptosis analysis, 2 $x10^5$ cells were plated in a 6-well culture plate and grown for 24 h. After 0.1,1,4,10 ug/ml Ag_{148} were added to the medium and incubated for 12 h, cells were digested with trypsin, washed once with cold PBS and resuspended in 1x binding buffer. The Annexin V/PI Apoptosis Detection Kit (BBI) was employed for apoptosis analyses according to the manufacturer's instructions.

Confocal fluorescence images

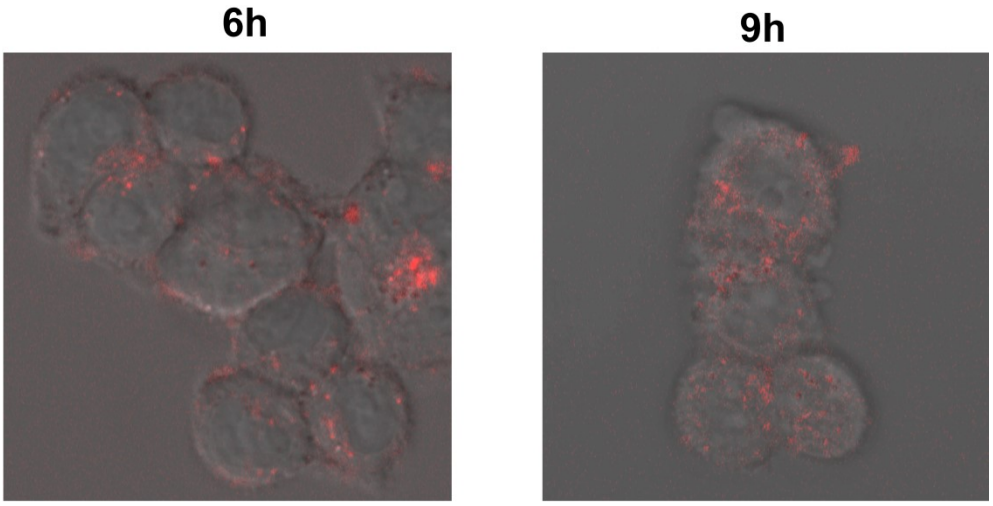

Figure S40. Confocal luminescence images of living HeLa cells incubated with Ag_{148}.

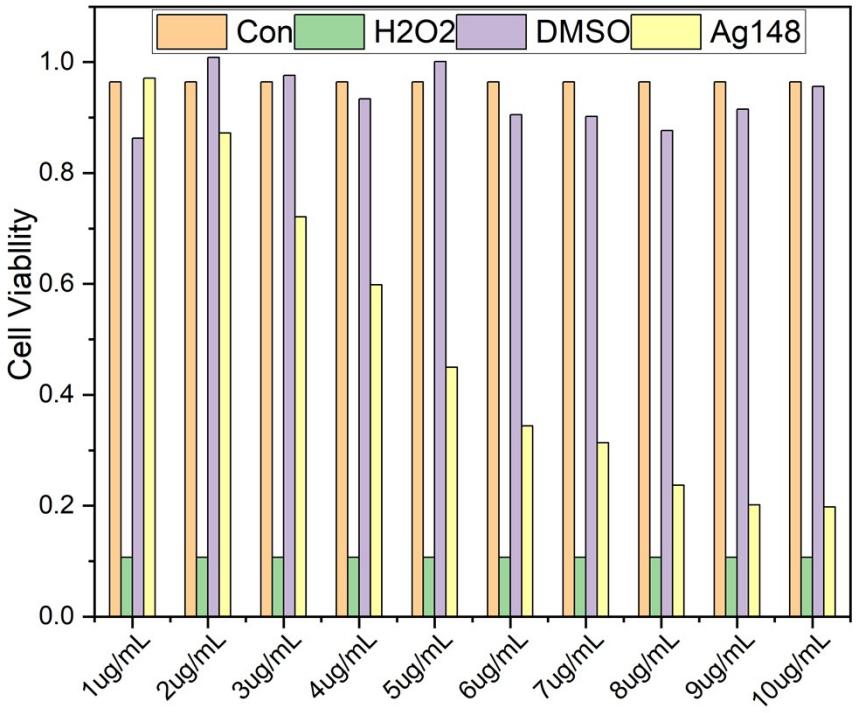

Figure S41. Toxicity assessment of 16HBE (normal lung epithelium) as healthy cells after treatment with Ag_{148} by MTT assays.

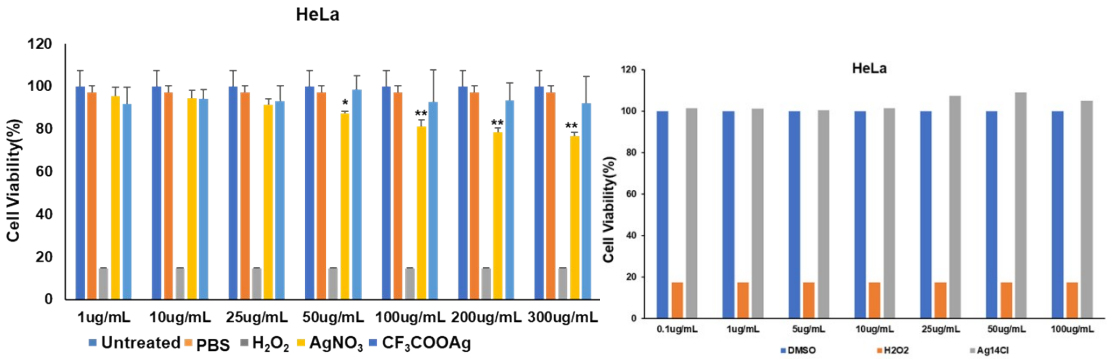

Figure S42. Toxicity assessment of HeLa cells after treatment with $AgNO_3$, CF_3COOAg and $Ag_{14}Cl$ by MTT assays.

Refrences

1. Sheldrick, G. M. *SHELXL-2014 Program for Crystal Structure Solution and Refinement, (University of Göttingen, Göttingen, Germany,* **2014***).*

2. Vandersluis, P.; Spek, A. L. *Acta Crystallogr. A.* **1990**, *46*, 194.

3. Dolomanov, O. V.; Bourhis, L. J.; Gildea, R. J.; Howard, J. A. K.; Puschmann, H. OLEX2: a complete structure solution, refinement and analysis program. J. Appl. Crystallogr. 2009, 42, 339-341.

4. Chen, Z.-Y.; Tam, D. Y. S.; Mak, T. C. W. Ethynide-Stabilized High-Nuclearity Silver(I) Sulfide Molecular Clusters Assembled Using Organic Sulfide Precursors. Chem. Commun. 2016, 52 (36), 6119.

5. Chen, Z.-Y.; Tam, D. Y. S.; Mak, T. C. W. Chloride Assisted Supramolecular Assembly of a Luminescent Gigantic Cluster: [Ag216S56Cl7(CCPh)98(H2O)12]- with pseudo-Th Skeleton and Five-Shell Arrangement. Nanoscale 2017, 9 (26), 8930.

6. Su, Y.-M.; Su, H.-F.; Wang, Z.; Li, Y.-A.; Schein, S.; Zhao, Q.-Q.; Wang, X.-P.; Tung, C.-H.; Sun, D.; Zheng, L.-S. Three Silver Nests Capped by Thiolate/Phenylphosphonate. Chem. Eur. J. 2018, 24 (56), 15096-15103.

7. Su, Y.-M.; Liu, W.; Wang, Z.; Wang, S.-A.; Li, Y.-A.; Yu, F.; Zhao, Q.-Q.; Wang, X.-P.; Tung, C.-H.; Sun, D. Benzoate-Induced High-Nuclearity Silver Thiolate Clusters. Chem. Eur. J. 2018, 24 (56), 4967-4972.

8. Nan, Z.-A.; Wang, Y.; Chen, Z.-X.; Yuan, S.-F.; Tian, Z.-Q.; Wang Q.-M. Catalyzed Assembly of Hollow Silver-Sulfide Cluster Through Self-Releasable Anion template. Commun. Chem. 2018, 99.

9. Sun, D.; Wang, H.; Lu, H.-F.; Feng, S.-Y.; Zhang, Z.-W.; Sun, G.-X.; Sun, D.-F. Two Birds with One Stone: Anion Templated Ball-Shaped Ag 56 and Disc-Like Ag 20 Clusters. Dalton Trans. 2013, 42 (18), 6281.

10. Xie, Y.-P.; Jin, J.-L.; Lu, X.; Mak, T. C. W. High-Nuclearity Silver Thiolate Clusters Constructed with Phosphonates. Angew. Chem., Int. Ed. 2015, 54 (50), 15176-15180.

11. Li, G.; Lei, Z.; Wang, Q.-M. Luminescent Molecular Ag-S Nanocluster [Ag62S13(SBut)32](BF4)4 . J. Am. Chem. Soc. 2010, 132 (50), 17678-17679.

12. Wang, Z.; Su, H.-F.; Wang, X.-P.; Zhao, Q.-Q.; Tung, C.-H.; Sun, D.; Zheng, L.-S. Johnson Solids: Anion-Templated Silver Thiolate Clusters Capped by Sulfonate. Chem. Eur. J. 2018, 24 (7), 1640-1650.

13. Cheng, L.-P.; Wang, Z.; Wu, Q.-Y.; Su, H.-F.; Peng, T.; Luo, G.-G.; Li, Y.-A.; Sun, D.; Zheng, L.-S. Small Size yet Big Action: a Simple Sulfate Anion Templated a Discrete 78-Nuclearity Silver Sulfur Nanocluster with a Multishell Structure. Chem. Commun. 2018, 54 (19), 2361.

14. Jin, J.-L.; Xie, Y.-P.; Cui, H.; Duan, G.-X.; Lu, X.; Mak, T. C. W. Structure-Directing Role of Phosphonate in the Synthesis of High-Nuclearity Silver(I) Sulfide-Ethynide-Thiolate Clusters. Inorg. Chem. 2017, 56 (17), 10412-10417.

15. Su, Y. M.; Wang, Z.; Schein, S.; Tung, C. H.; Sun, D. A Keplerian Ag 90 Nest of Platonic and Archimedean Polyhedra in Different Symmetry Groups. Nat. Commun. 2020, 11, 3316.

16. Deng, C.-L.; Sun, C.-F.; Wang, Z.; Tao, Y.-W.; Chen, Y.-L.; Lin, J.-Q.; Luo, G.-G.; Lin, B.-Z.; Sun, D.; Zheng, L.-S. A Sodalite-Type Silver Orthophosphate Cluster in a Globular Silver Nanocluster. Angew. Chem. Int. Ed. 2020, 59 (31), 12659-12663.

17. Su, Y.-M.; Wang, Z.; Tung, C.-H.; Sun, D.; Schein, S., Keplerate Ag192 Cluster with 6 Silver and 14 Chalcogenide Octahedral and Tetrahedral Shells. J. Am. Chem. Soc. 2021, 143 (33), 13235-13244